CaMKII binds both substrates and activators at the active site

Can Özden[1,2], Roman Sloutsky[1], Tomohiro Mitsugi[5], Nicholas Santos[1], Emily Agnello[1], Christl Gaubitz[4], Joshua Foster[2], Emily Lapinskas[1], Edward A. Esposito[3], Takeo Saneyoshi[5], Brian A. Kelch[4], Scott C. Garman[1], Yasunori Hayashi[5], Margaret M. Stratton[1]†

[1]Department of Biochemistry and Molecular Biology, University of Massachusetts, Amherst, MA 01003, USA. [2]Molecular and Cellular Biology Graduate Program, University of Massachusetts, Amherst, MA 01003, USA. [3]Malvern Panalytical, Northampton, MA 01060, [4]Department of Biochemistry and Molecular Biotechnology, University of Massachusetts Chan Medical School, Worcester, MA 01605, USA. [5]Department of Pharmacology, Kyoto University Graduate School of Medicine, Kyoto, Japan.

† Corresponding author. Email: mstratton@umass.edu (M.M.S.)

ABSTRACT

Ca^{2+}/calmodulin dependent protein kinase II (CaMKII) is a signaling protein that is required for long-term memory formation. Ca^{2+}/CaM activates CaMKII by binding to its regulatory segment, thereby freeing the substrate binding site. Despite having a large variety of interaction partners, the specificity of CaMKII interactions have not been structurally well-characterized. One exceptional feature of this kinase is that interaction with specific binding partners persistently activates CaMKII. To address the molecular details of this, we solved X-ray crystal structures of the CaMKII kinase domain bound to four different binding partners that modulate CaMKII activity in different ways. We show that all four partners bind in the same manner across the substrate binding site. We generated a sequence alignment based on our structural observations, which revealed conserved interactions. Using biochemistry and molecular dynamics simulations, we propose a mechanistic model that persistent CaMKII activity is facilitated by high affinity binding partners, which compete with the regulatory segment to allow substrate phosphorylation.

INTRODUCTION

Ca^{2+}/calmodulin-dependent protein kinase II (CaMKII) is a central signaling protein that controls various cellular functions such as synaptic plasticity, cytoskeletal regulation, cell growth and division, gene transcription and ion channel modulation [1]. CaMKII biology has been an active focus of research especially because of its crucial role in long-term potentiation (LTP), which is the basis for long-term memory [2, 3]. CaMKII is highly abundant in the forebrain postsynaptic density (PSD) fraction, where it makes up to 2% of total protein [4]. CaMKII is a multisubunit complex made up of 12-14 subunits, which is oligomerized by the hub domain (**Fig. 1a**). Each CaMKII subunit contains a Ser/Thr kinase domain, autoinhibitory/regulatory segment, variable linker region, and a hub domain (**Fig. 1b**). LTP is governed by many molecular interactions, including dozens with CaMKII, however the structural details of these interactions are lacking (**Fig. 1c**) [5].

Ca^{2+}/calmodulin (Ca^{2+}/CaM) activates CaMKII by binding to the regulatory segment and thereby freeing the substrate binding site. This well-understood mechanism triggers trans-autophosphorylation of T286, which renders CaMKII constitutively active until T286 is dephosphorylated. CaMKII has also been shown to maintain activity in the absence of Ca^{2+}/CaM and T286 phosphorylation by another mechanism that invokes two binding partners [6-9], for which we lack a clear mechanism. There are two binding partners (NMDA receptor and Tiam1) that have been shown to be activators of CaMKII after the Ca^{2+} stimulus dissipates, with

or without T286 phosphorylation [7-9]. The GluN2B subunit of the NMDA receptor is a known substrate of CaMKII [10, 11], and to this point, the best studied CaMKII activator [12]. Ca^{2+}/CaM-activated CaMKII has been shown to form a persistent complex with GluN2B, which locks CaMKII in an active conformation, as long as binding persists [7, 11]. To date, persistent binding of CaMKII to GluN2B and resultant activation has been explained by a hypothetical model [8]. In this model, GluN2B first binds to Ca^{2+}/CaM-activated CaMKII close to the active site (termed S-site), presenting Ser 1303 for phosphorylation. Then, GluN2B stays persistently bound at the base of the CaMKII C-lobe, away from the active site (termed T-site), while freeing the S-site to bind and phosphorylate other substrates. This model has been widely accepted in the field, but to date, there is no structural data supporting it.

Another known activator is Tiam1, a Rac guanine-nucleotide exchange factor (RacGEF), and it is phosphorylated multiple times by CaMKII. The carboxy tail of Tiam1 also forms a stable complex with CaMKII using a pseudosubstrate sequence (alanine at the phosphorylation site). This Tiam1:CaMKII interaction leads to reciprocal activation of Tiam1 and CaMKII in a complex known as the reciprocally activating kinase-effector complex (RAKEC) [9]. On the other hand, Densin-180 (LRRC7) is a postsynaptic scaffolding protein. It also forms a stable complex with CaMKII through a pseudosubstrate sequence (Ile at the phosphorylation site), but unlike GluN2B or Tiam1, it inhibits kinase activity [13, 14]. Finally, the AMPA receptor subunit GluA1 is a CaMKII substrate but not a known activator [15, 16]. GluA1 phosphorylation by CaMKII is important for synaptic plasticity [17-19].

In the current study, we solved new co-crystal structures of the CaMKII kinase domain bound to peptides from GluN2B, Tiam1, Densin-180, and GluA1. Using these structures as starting points, we compared molecular dynamics (MD) simulations of the kinase domain in complex with GluN2B, Tiam1, and a previously solved structure with CaMKII bound to an inhibitor, CaMKIIN1 [20]. Combining this structural information and observations obtained from MD simulations with the biophysical and biochemical measurements has allowed us to clarify important interactions that drive binding and propose a working model for maintaining CaMKII activity in the absence of Ca^{2+}/CaM.

RESULTS

The studies outlined below include characterization of peptides from the following five binding partners: GluN2B (residues 1289-1310), GluA1 (residues 818-837), Densin-180 (residues 797-818), and Tiam1 (residues 1541-1559). We also include CaMKIIN1 (residues 37-58) in these studies, which is a known endogenous inhibitor of CaMKII [21-23]. Unless otherwise specified, all experiments were conducted in the background of an inactivating CaMKII mutation (D135N).

CaMKII kinase domain interacts similarly with different binding partners

We used a fluorescence polarization (FP) assay to measure binding of the CaMKII kinase domain to the five peptides listed above. Four out of five peptides bound to the kinase with similar affinities, where K_d values ranged from 1.3 μM to 4.5 μM (GluN2B K_d = 1.3±0.05 μM, CaMKIINtide K_d = 2.9±0.23 μM, Densin-180 K_d = 3.4±0.22 μM, and Tiam1 K_d = 4.5±0.43 μM) (**Fig. 2b**). The one exception was GluA1, which bound with a significantly lower affinity (K_d = >50 μM) (**Fig. 2b**). FP measurements require the addition of a fluorophore to the peptide as well as a small amount of detergent to avoid nonspecific interactions with the fluorophore. To obtain binding energetics in the absence of a fluorophore and detergent, we used isothermal titration calorimetry (ITC). These measurements also revealed similar affinities across peptides except for GluA1. The K_d values calculated from ITC were significantly lower for the tight binders, ranging from 56 nM – 1.15 μM (GluN2B K_d = 128±18.3 nM CaMKIIN2 K_d = 56±12.5 nM, Densin-

180 K_d = 666±91.1 nM, Tiam1 K_d = 1.15±0.09 μM) (**Fig. S2, Table S1**). The reason for the difference between the two methods is likely that binding is tighter in the absence of detergent and bulky aromatic groups from the fluorophore. In contrast, GluA1 consistently had a significantly lower affinity (K_d >66 μM).

We solved 13 total crystal structures of the kinase domain of CaMKII with the active site occupied by a nucleotide ligand or empty and bound to one of four peptides: GluN2B, GluA1, Densin-180, and Tiam1 (**Fig. 2, S1**). All structures have resolutions within the range of 1.85 - 2.7 Å (**Table 1, 2**).

We solved nine structures of the CaMKII kinase domain bound to the GluN2B peptide. The first two structures are the WT kinase domain bound to WT GluN2B peptide, one with ADP in the active site (PDB:6XDU) and one with an empty nucleotide binding pocket (PDB:6XDL). The next two structures are the D135N kinase domain bound to WT GluN2B peptide with either ATP (PDB:6XBX) or methyl 6-O-(N-heptylcarbamoyl)-alpha-D-glucopyranoside (hecameg) (PDB:6XBP) in the nucleotide binding pocket. The other five structures are the D135N kinase domain bound to the phosphomimetic GluN2B peptide (S1303D). Two of these structures have ATP bound in the nucleotide binding pocket (PDB:7KL1,6XOE) and two have empty nucleotide binding pockets (PDB:7KL4,7KL2), all four of these had different unit cell dimensions. The 5th structure has hecameg bound in the nucleotide binding pocket (PDB:7KL0). In all nine structures, we observed that the interaction between the GluN2B peptide and the kinase domain is identical.

We solved two structures of the kinase domain bound to the Tiam1 peptide, one with ATP in the nucleotide binding pocket (PDB:6XFO) and one with an empty nucleotide binding pocket (PDB: 6X8V). Finally, we solved structures of the kinase domain bound to the Densin-180 peptide (PDB:6X5G) and the GluA1 peptide (PDB:6X5Q), both with empty nucleotide binding pockets.

Across all 13 structures, we observed that all peptides interacted with the same surface on the kinase domain. The overall fold of the kinase domain is similar in all structures with a range of Cα RMSD values from 0.583 - 1.611 Å. We resolved 14-19 residues in each peptide (**Fig. 2a, S1**). GluN2B and Densin-180 peptides bound in completely extended conformations across the substrate binding site. Tiam1 and GluA1 peptides adopted short helical turns, similar to what was previously observed in the CaMKIINtide structure [20]. Additionally, Densin-180 forms an intrachain electrostatic interaction between the -3 position arginine and upstream aspartate (numbering is based on the prototypical GluN2B substrate with the phosphorylation site set to zero).

Sequence alignment of CaMKII binding partners based on high-resolution structures

So far, predicting CaMKII interaction partners has been difficult due to conformational heterogeneity in binding. For example, our structures revealed that several peptides have helical turns, which shifted the register of conserved interactions (Tiam1, GluA1, and the previously observed CaMKIINtide). We now provide an updated sequence alignment based on our structural observations (**Fig. 2c**). The two peptides that are substrates (GluN2B and GluA1) have the phosphosite facing the nucleotide binding pocket, such that both peptides are docked at the active site, ready to be phosphorylated. The critical residues of the binding partner mediating this interaction are conserved at positions +1, -2, -3, -5, and -8, as discussed below (**Fig. 2c**).

153 **Conserved hydrophobic interactions**
154
155 Interactions at the +1 position. We observed in our structures that a small hydrophobic residue
156 is preferred at the +1 position, which has been previously noted [24-28] (**Fig. 2c**). In all
157 structures, backbone atoms of the +1 position residue hydrogen bonds with the backbone of
158 G175 (**Fig. 3**). Adjacent to G175, there is a hydrophobic patch formed by F173, P177, L185,
159 and Y222. GluA1, CaMKIIN, and Densin-180 all have Val or Ile at the +1 position, which are
160 buried in this hydrophobic groove. In GluN2B and Tiam1, Tyr and Leu, respectively, occupy this
161 position and face out of the groove. Tyr is too large and polar to favorably interact with the
162 groove. Leu is the C-terminal residue on the Tiam1 peptide which may be why it does not stably
163 interact with the groove in the structure, which is discussed further below.
164
165 We performed MD simulations of the kinase domain in complex with extended versions of
166 peptides from GluN2B (1263-1328, adding 32 N-terminal residues and 20 C-terminal residues)
167 and Tiam1 (1513-1581, adding 28 N-terminal residues and 22 C-terminal residues) and the full-
168 length CaMKIIN1 protein (adding 41 N-terminal residues and 22 C-terminal residues). In these
169 simulations, extended peptides interact via two residues (+1 and +4 positions in NR2B and
170 Tiam1, +1 and +2 in CaMKIINtide; **Fig. S3f-h**) with the hydrophobic patch formed by F173,
171 P177, L185, and Y222. The +1 leucine and +4 isoleucine of Tiam1 pack with the four kinase
172 residues into a stable conformation, with pairwise RMSD of less than 2 Å – meaning that
173 between any two frames in the simulation, the RMSD of these atoms is lower than 2 Å (**Fig.**
174 **S3f**). The interaction is more fluid for GluN2B and CaMKIIN1, but their respective residues
175 remain in close proximity to the patch throughout the trajectory (**Fig S3g, h**).
176
177 Hydrophobic interaction at the -5 position. All CaMKII interactors studied here have a conserved
178 leucine residue at the -5 position, which fits into a hydrophobic pocket on the kinase domain
179 comprised of F98, I101, V102, and I205 (**Fig. 3, 4a**). In our structures, leucine is 3.3-4.5 Å from
180 the four hydrophobic residues, indicating a tight interaction. In the CaMKIINtide structure, a turn
181 motif is facilitated by two glycine residues, which orients the leucine into this pocket [20]. In
182 simulations of GluN2B, Tiam1, and CaMKIINtide, this interaction also demonstrates high
183 structural integrity, with pairwise RMSD below 2 Å (**Fig. 4b**).
184
185 Docking site mediated by W214. In both Densin-180 and CaMKIINtide structures, the
186 sidechains of proline and isoleucine (highlighted blue in **Fig. 2c**) pack against W214 on the
187 kinase domain (**Fig. 4c**). Additionally, for Densin-180, the guanidino group of R808 at the -7
188 position hydrogen bonds with the backbone carbonyl group of W214 and the sidechain of Q224.
189 In simulations of CaMKIIN1, W214 and Q224 interact persistently, with pairwise RMSD below
190 1.5 Å (**Fig. 4e**). In the simulation of Tiam1 bound to the kinase domain, the leucine at position
191 -14 moves to form a persistent interaction with W214 (**Fig. 4c, e**, highlighted blue in **Fig. 2c**).
192 However, in the Tiam1 crystal structure, this leucine is close to the N-terminus, which interacts
193 with another monomer in the asymmetric unit, pulling the leucine >13 Å from W214 in one
194 monomer, and it is not resolved in the other monomer.
195
196 We used FP to measure the effect on peptide binding to a kinase domain harboring a mutation
197 at this tryptophan (W214A). The W214A mutation complete abolished CaMKIINtide binding,
198 whereas the effects on the other binding partners were not as severe (2- to 4-fold decreased
199 affinity) (**Fig. 4d, S3a, b, c**). Although both CaMKIINtide and Densin-180 structures show an
200 interaction with W214, mutation at this site dramatically decreased CaMKIINtide binding
201 completely but only had a marginal effect on Densin-180 binding (**Fig. 4d**). CaMKIINtide
202 docking onto W214 likely stabilizes its helical motif, which properly orients the -5 leucine into the
203 hydrophobic pocket. When W214 is mutated, this interaction is disrupted and the -5 leucine

interaction is unlikely to be maintained in CaMKIINtide, completely disrupting binding. Densin-180 does not have a helical motif, which may explain why the W214A mutant does not have a drastic effect.

Electrostatic interactions provide specificity

Ionic interactions at the -2 position. Glutamine is commonly at the -2 position of CaMKII interactors [24-26, 28]. Indeed, all four peptides in our structures have glutamine at -2, allowing us to resolve the important interactions mediated by both the backbone and the sidechain at this position (**Fig. 3**). The -2 glutamine sidechain amide oxygen forms a hydrogen bond with the backbone of G178, and the amino group interacts with the sidechain of Y179. The backbone carbonyl interacts with sidechain of K137, and the backbone amino group interacts with E139, which has also been shown to be important for binding (**Fig. S4, S4j**) [8]. Of note, CaMKIINtide has a serine at the -2 position instead of glutamine (**Fig. 2c**). In this structure, the serine sidechain is flipped relative to glutamine, which enables hydrogen bonding with E139 and K137 sidechains [20]. This observation is consistent with a previous study, which showed that CaMKIINtide binding to CaMKII was reduced when this serine was mutated to alanine [29].

Conserved salt bridge close to the active site. The -3 position is a conserved basic residue, arginine or lysine, which interacts with conserved glutamate residues on the kinase domain [20, 30]. In the crystal structures, all interactors except for low-affinity binder GluA1 have a basic residue at the -3 position, which forms salt bridges with two glutamic acid residues (E96, E99) located on the αD helix of the kinase domain (**Fig. 3, 5a**). The basic residues of interaction partners are positioned 2.4 – 4.2 Å between E96 and E99. In the Densin-180 and CaMKIINtide structures, the -3 arginine is closer to E96, whereas in the Tiam1 structure, the -3 lysine is closer to E99. In the structures of GluN2B, the -3 position is either more closely associated with E96 (PDB:6XDL, WT kinase with empty active site; PDB:6XDU, WT kinase with ADP bound) or E99 (PDB:6XBP, D135N kinase with a detergent bound; PDB:6XBX, D135N kinase with ATP bound) (**Fig. S4a**). Additionally, in structures where ATP/Mg is also bound (GluN2B, Tiam1), the side chain of E96 interacts with the hydroxyl group of ribose in the ATP molecule (3.7 – 4.3 Å; **Fig. S4d**) [31]. These salt bridges are not formed in the GluA1 interaction, because there is a proline at the -3 position (**Fig. 2c**). In the GluA1 structure, the sidechain of E96 is flipped away from the peptide compared to the other four structures where it is oriented toward the binding partner (**Fig. 5a**, inset). Additionally, the sidechain of E99 is not as well-resolved in the GluA1 structure.

We hypothesized that the reason for GluA1's lower affinity compared to other interaction partners is due to the lack of this salt bridge. To test this, we created charge reversal mutations (E→K), and also E→Q mutations that maintain the possibility of hydrogen bonding, but not the electrostatic component. We directly compared binding affinities of GluN2B (which has a basic residue at the -3 position) to GluA1 which is lacking this interaction. Single E96K and E99K mutations were more disruptive to GluN2B binding (affinity decreased 7- and 5-fold, respectively) compared to GluA1 binding (affinity decreased <2-fold) (**Fig. 5b, c**). The double lysine mutation (E96/99K) significantly reduced the binding affinity for GluN2B peptide 52-fold (K_d = 68.7±33.7 μM), while the affinity for GluA1 was roughly the same. In contrast, the E→Q mutations were less disruptive to binding. GluN2B binding to E96Q and E99Q was only marginally impaired (affinity decreased <2-fold), while the binding affinity of GluN2B for the double mutant E96/99Q was weakened by ~4-fold (K_d = 5±0.31 μM) (**Fig. S4b**). All glutamine mutants showed similar binding to GluA1 compared to WT, where the binding affinities were >73 μM (**Fig. S4c**). The double glutamine mutant (E96/99Q) expressed more poorly than WT,

but the double lysine mutant (E96/99K) reduced the protein expression significantly, likely due to destabilization.

In simulations, the -3 residue also forms a persistent interaction with E139. The -3 arginine of GluN2B forms 2-4 ionic interactions nearly 100% of the time, mostly with E96 and E139 (**Fig. S4g)**, while the lysine of Tiam1 forms 1-2 ionic interactions ~70% of the time, mostly with E139 (**Fig. S4h**). There are no observed interactions between the ATP phosphate groups and the GluN2B and Tiam1 chains. The interactions observed in the CaMKIIN1 trajectories were very different. The arginine at the -3 position mostly interacts with E139, minimally with E96, and not at all with E99 (**Fig. S4i**). The arginine residues at the 0 and -3 positions form very stable contacts with the ATP phosphates, which locks the ATP in an altered position (**Fig. S4e, j**). This conformational change precludes the ATP adenosine from forming ionic interactions with the backbones of D90 and V92, as observed in the crystal structure. As a result, the ATP adenosine group exits the binding pocket in the CaMKIIN1 trajectories (**Fig. S4e**). In these trajectories, the serine at the -2 position of CaMKIINtide forms a hydrogen bond with E139 ~98% of the time (**Fig. S4j**), whereas in GluN2B and Tiam1 trajectories, the glutamine at the -2 position does not form stable interactions.

We performed FP measurements comparing binding of CaMKIINtide to the kinase domain with charge reversal mutations (E96K, E99K), with and without ATP (**Fig. S4f**). In the absence of ATP, E96K and E99K both have a ~9-fold reduced binding affinity to CaMKIINtide. MD trajectories would predict that CaMKIIN1 binding is facilitated by E96 in the presence of ATP, whereas E99 plays essentially no role. Consistent with this, ATP binding restored E99K binding to that of WT (D135N), whereas the affinity of E96K was still weakened.

<u>Salt bridge at the base of the C-lobe.</u> We observed a conserved basic residue at the -8 position (arginine or lysine) mediating a salt bridge with E236 on the kinase domain (**Fig. 2c, 3, 6a**). This likely has not been fully characterized because this position is quite far from the phosphorylation site (~30 Å), and substrate alignments have not been accurate enough to highlight the conservation at this position. We tested the effect of mutating E236 to lysine (E236K) on binding affinity using FP. The E236K mutation completely abolished Tiam1 and GluA1 binding (**Fig. 6b, S5b**). For Densin-180 and GluN2B, E236K binding affinity was reduced ~6-fold (K_d = 21±2.01 μM) and ~7-fold (K_d = 9.1±1.27 μM), respectively (**Fig. S5a, S5c)** [8].

We investigated whether peptide phosphorylation influences binding affinity by measuring the affinity of D135N and D135N/E236K to the GluN2B peptide harboring a phosphomimetic substitution (S→D at position 0). There was very little effect on the phosphomimetic GluN2B binding to D135N (K_d = 2.1±0.07 μM), whereas affinity for the E236K mutant was reduced ~14-fold (K_d = 28±13 μM) (**Fig. S5d**). For CaMKIINtide, binding affinity was drastically reduced in our FP measurement (**Fig. S5e**). However, we performed an ITC experiment using full length CaMKIIN2 and observed a tight binding constant (K_d = 951±160 nM) (**Fig. S2f**). Since we observed a dramatic difference (~50-fold) between FP and ITC data in D135N CaMKII binding measurements, it is possible that the detergent is more detrimental to CaMKIIN2 binding compared to other interactions. This, as well as the favorable entropic term from our ITC measurements (**Table S1**), is in line with our observation of multiple hydrophobic interactions being important for this very tight binding inhibitor. A previous study tested the inhibitor efficacy of CaMKIINtide by doing alanine scanning. When the Arg that interacts with E236 in the crystal structure was mutated, the interaction was not fully disrupted and CaMKII gained ~10% activity back [29].

We investigated the role of E236 in the MD trajectories, which revealed an additional interaction. In addition to interacting with the -8 position, E236 also forms a persistent hydrogen bond with the hydroxyl group of Y210, thereby locking the Y210 side chain into a persistent interaction with W237 with very high structural integrity (RMSD <0.75 Å) (**Fig. S5f, j-l**). We performed simulations of GluN2B and Tiam1 complexes with an E236K mutation, which showed that the interaction between Y210 and W237 is disrupted by the loss of the hydrogen bond with Y210 (**Fig. S5k, l**). The resulting movements of the Y210 side chain disrupt the W214 interaction with Tiam1, which may explain the loss of binding. In GluN2B, the interaction between Y210 and W237 is also disrupted, but the -8 arginine of GluN2B switches to a highly persistent interaction with D231.

Interrogating CaMKII interactions with full-length binding partners

We used a pull-down assay to assess the effect of CaMKII mutations on interactions with full-length binding partners. We co-transfected HEK293 cells with FLAG-tagged CaMKIIα and either full-length Tiam1, GluN2B, or GFP-CaMKIIN2. Binding was assessed by western blot following immunoprecipitation with an anti-FLAG antibody. Immunoprecipitation with E236K showed a remarkable loss of binding for both Tiam1 and GluN2B, similar to our FP data (**Fig. 6d, S6a**). E236K CaMKII resulted in better binding to CaMKIIN2 compared to WT CaMKII in HEK293 cells (**Fig S6b**). Our ITC results showed tight binding between E236K CaMKII kinase domain and CaMKIIN2, and it is known that the E236K mutation disrupts the regulatory segment from binding [30], thereby facilitating more CaMKIIN binding to E236K compared to WT since the binding site is more available.

The immunoprecipitation experiments corroborate our peptide binding data that show the importance of hydrophobic interactions. Indeed, mutating the hydrophobic pocket at the -5 position (I205K) showed significant loss of CaMKII binding to Tiam1, GluN2B, and CaMKIIN2 (**Fig. 6d, S6**). Finally, the W214A mutation also disrupted binding to Tiam1, GluN2B, and CaMKIIN2. Consistent with our FP data, CaMKIIN2 binding to W214A is nearly abolished (**Fig. S6b**). We observed a subtle effect on W214A binding the peptide of Tiam1 in our FP assay, however using full-length Tiam1 in the pull-down revealed a significant effect on binding with less than 25% relative binding compared to WT (**Fig. 6d, e**). This reflects what we observed in the simulation using the longer Tiam1 peptide (**Fig. 4c**). Finally, the W214A mutation weakened the interaction with full-length GluN2B by ~40%, similar to what we observed in our FP measurements (**Fig S6a**).

Testing the 2-site binding model

We wanted to directly test the idea of the 2-site binding model (S- and T-sites) [8]. Previous studies have shown that GluN2B peptide could not be competed off by Syntide-2 even at millimolar concentrations, which we also observed (**Fig. 6c**) [11]. As noted by Colbran and colleagues [11], a sequence alignment of Syntide-2 and other substrates reveals that the Syntide-2 peptide is shorter and therefore missing the -8 position basic residue we discuss above (**Fig. 6c**). To test whether this is the reason Syntide-2 could not compete GluN2B, we created an extended version of Syntide-2 by adding three residues to the N-terminus, mimicking Densin-180. The extended version of Syntide-2 did compete off GluN2B (K_i ~ 78±13.6 μM) (**Fig. 6c**). This result shows that Syntide-2 and GluN2B do occupy the same binding site, indicating that there are not two separate binding sites on the kinase domain.

If there are not two binding sites, how is CaMKII activity maintained by specific binding partners like GluN2B? The mode of activation must invoke the phosphorylated form of GluN2B since this is observed under activating conditions. In a canonical kinase reaction, the kinase first binds substrate, then transphosphorylation occurs, and finally the substrate is released. We measured

355 the affinity of a phosphomimetic version of GluN2B (S1303D) and observed only a 7-fold
356 reduction in affinity (K_d = 919±100 nM) compared to unphosphorylated GluN2B (K_d = 128±18.3
357 nM) (**Fig. S2a, g**). We were also able to crystallize the kinase domain bound do GluN2B
358 S1303D (Table 1), which showed a very similar conformation to WT GluN2B. We hypothesized
359 that phospho-GluN2B would act as a competitive inhibitor with Syntide-2. We performed
360 coupled-kinase assays using Syntide-2 as a substrate in the presence of saturating GluN2B
361 S1303D. As a control, we also measured activity against Syntide-2 in the presence of the
362 CaMKIIN2 inhibitor. Indeed, high levels of CaMKIIN2 inhibit Syntide-2 phosphorylation, whereas
363 GluN2B acts as a competitive inhibitor, exemplified by comparable V_{max} values but an increased
364 K_m value (**Fig. 7a**).
365
366 **Generalizing CaMKII binding partners**
367 We mined the curated database of CaMKII phosphorylation sites (n=418) for consistencies with
368 our updated alignment and found additional similarities (**Fig. S7**, www.phosphosite.org).
369 Hydrophobic residues (I, V, L, M, F) are found at +1, Q is found at -2, and R is overwhelmingly
370 found at -3, but also at -2 and -4. Smaller hydrophobic residues (L, V, I or M) are found at -5 and
371 -6. Generally, the minus direction disfavors P, D, and E. In contrast, acidic residues D and E are
372 highly favored at +2. GluN2B has D at the +2 position, and we note an interaction with K56 in
373 several structures, which was also observed in the *d*EAG-bound structure (PDB: 5H9B) (**Fig.
374 2C**). In addition, S, which may serve as a second phosphorylation site, is strongly disfavored at
375 nearly every position [28].
376
377 **DISCUSSION**
378 CaMKII has a broad range of substrates and interaction partners. CaMKII recognizes a
379 consensus sequence R-X-X-S/T, yet the structural details driving these interactions had not
380 been elucidated. We addressed this by solving co-crystal structures of four binding partners
381 bound to the CaMKII kinase domain, which allowed us to highlight the interactions mediating
382 binding. Like many kinases, CaMKII prefers a basic residue at the -3 position [32]. Our crystal
383 structures, along with others [20, 31], show an electrostatic interaction between the -3 position
384 and E96/E99. E96 is well-conserved across kinases and known to be important for ATP binding
385 (**Fig. S7a, S4d**) [31]. E99 is not as well-conserved, even across other CaM-kinases, indicating
386 that it is not as crucial for ATP binding (**Fig. S7a, c, d**) [33]. Our MD simulations showed E139
387 interacting with the -3 position (**Fig. S4g-j**). Previous studies have shown that mutations at E139
388 have a negative effect on AC-2 and GluN2B binding [8, 30]. The simulations also show the 0
389 and -3 positions of CaMKIIN1 (both Arg) strongly interact with ATP. Further efforts will
390 interrogate the role of ATP coordination in CaMKIINtide inhibition. The biological ramifications of
391 the weak interaction between CaMKII and GluA1 will need to be further investigated – where
392 localization of CaMKII to this receptor by another factor or avidity effects of holoenzyme
393 localization may be driving GluA1 phosphorylation *in vivo* [37]. Our observation might explain
394 the molecular basis of a recent study that reported lower levels of S831 phosphorylation in the
395 hippocampus [38].
396
397 Upon CaMKII activation, the αD helix reorients outward, exposing a hydrophobic pocket for
398 substrate binding, which we observed in all our structures at the -5 position. Kuriyan and
399 colleagues first identified this hydrophobic pocket as 'docking site B', which is comprised of
400 residues F98, I101, V102, and I205 [20]. Previously, F98 has been reported as part of the 'S-
401 site' and I205 has been reported as part of the 'T-site' [8, 30]. However, it is clear from
402 structures that these residues comprise the same binding site (**Fig. 3, 4a**). This hydrophobic
403 pocket is highly conserved across CaM-kinases, but not other kinases (**Fig. S7a**). If we compare
404 structures of a kinase domain with an empty substrate binding site (PDB:6VZK) to a kinase
405 domain bound to a substrate, it is clear that F98 and V102 undergo a conformational change in

the bound state to form the pocket (**Fig. S3d**). This indicates that these hydrophobic residues shift to accommodate substrate binding, which is likely a large contribution to an observed gain in kinase domain stability upon each binding (**Fig. S3e**), similar to what we have previously observed with regulatory segment binding, which is mediated by L290 in the regulatory segment [34].

In all crystal structures, we observed a salt bridge at E236 mediated by a basic residue at the -8 position. Similarly, in the crystal structure of the fly kinase domain bound to a *d*EAG peptide, there is a glutamine residue interacting with E236 [28]. In our pull-down assays, a significant loss of binding was observed for both Tiam1 and GluN2B (**Fig. 6d, S6a**). In the trajectory of E236K:GluN2B, the -8 arginine switches to interacting with D231, suggesting that this interaction may compensate for the E236K mutation. E236K is also unable to form the H-bond with Y210, making the tyrosine side chain more mobile in MD simulations, and disrupting the interaction between Tiam1 and W214. More work needs to be done to determine whether this electrostatic interaction provides specificity, which could be exploited in biological experiments.

Here, we propose a new mechanistic model for prolonged CaMKII activity in the presence of specific binding partners. Let's consider the mode of activation by GluN2B as the activator shown in **Figure 7b**. Phospho-GluN2B is a high affinity binder, and we hypothesize there is an intermediate step between product dissociation (Rxn 4) and regulatory segment re-binding (Rxn 5). As described, a conformational change is required for regulatory segment re-binding [34], which would allow substrate phosphorylation if the concentration were high enough (Rxn 7). In conditions where the activator concentration is high, activator rebinding will be favorable since this high affinity binder will have a relatively high on-rate and low off-rate. A submicromolar affinity for a kinase interaction partner/substrate is unique, as typically these interactions are in the K_d range of 200 μM [35]. GluN2B has the phosphorylatable serine (S1303) which is potentially a key regulator for this tight interaction as the phosphorylated version would typically have lower affinity, however in this case it is still sub-micromolar. Indeed, Colbran and colleagues has been shown that S1303A mutation renders GluN2B an inhibitor, indicating a very slow off-rate [36]. Tiam1 also allows maintenance of CaMKII activity and binds with low micromolar affinity, however, Tiam1 does not have a phosphorylatable residue. Perhaps these high affinity interactors allow these interaction partners to kinetically compete with the regulatory segment rebinding, yet they allow the enzyme to bind and phosphorylate other substrates. On the other hand, CaMKIIN binds with nanomolar affinity, which is what makes it a terminal inhibitor for CaMKII.

The crystal structures presented here provide clarity on the interactions between CaMKII and its binding partners, which will be crucial in guiding biological experiments to assess the downstream effects of specific interactions. These observations will be crucial in guiding further experiments, which will necessarily invoke the complexities of the CaMKII holoenzyme structure. It is intriguing to consider other enzymes that might be modulated in a similar way by high affinity binding partners as a novel mechanism for prolonged activation.

MATERIALS AND METHODS

Cloning

All CaMKIIα variants were expressed with an N-terminal His-SUMO tag in a pET vector. All point mutations were created using site-directed mutagenesis.

Protein Expression and Purification

WT CaMKIIα kinase domain (residues 7-274) was co-expressed with λ phosphatase in *E. coli* BL21(DE3). Inactive constructs (D135N) and CaMKIIN2 *(Rattus norvegicus)* were expressed without λ phosphatase. The cells were induced at 18 °C with 1 mM Isopropyl β- d-1-thiogalactopyranoside (IPTG) and grown overnight. Following to ~16 hours incubation, cell pellets were resuspended in Buffer A (25 mM Tris, pH 8.5, 50 mM KCl, 40 mM imidazole, 10% glycerol) and commercially available protease inhibitors (0.5 mM Benzamidine, 0.2 mM AEBSF, 0.1 mg/mL trypsin inhibitor, 0.005 mM Leupeptin, 1 µg/mL Pepstatin), 1 µg/mL DNAse/50 mM $MgCl_2$ were added, then lysed. All following purification steps were performed using an ÄKTA pure chromatography system at 4 °C. Filtered cell lysate was loaded onto a 5 mL His Trap FF NiNTA Sepharose column (GE), and eluted with 50% Buffer B (25 mM Tris-HCl pH 8.5, 150 mM KCl, 1 M imidazole, 10% glycerol). The protein was desalted from excess imidazole using a HiPrep 26/10 Desalting column using Buffer C (25 mM Tris-HCl pH 8.5, 40 mM KCl, 40 mM imidazole, 2 mM TCEP, 10% glycerol). His SUMO tags were cleaved with Ulp1 protease overnight at 4 °C. Cleaved His SUMO tags were separated by a subtractive NiNTA step prior to an anion exchange step. Proteins were eluted from HiTrap Q-FF with a KCl gradient. Eluted proteins were concentrated and further purified in gel filtration buffer (25 mM Tris-HCl pH 8.0, 150 mM KCl, 1 mM TCEP, 10% glycerol) using Superdex 75 10/300 GL size exclusion column. Fractions (>95% purity) were pooled, concentrated, aliquoted and flash frozen in liquid nitrogen, and stored at -80 °C until needed.

Peptide synthesis

Peptides used for co-crystallization were synthesized and amidated at the C-terminus (Genscript, RIKEN Research Resource Center). Peptides used for fluorescence polarization assays were synthesized with an additional N-terminal 5-FAM.

Full length peptide sequences are as follows:
Human GLUA1 (residues 818-837): SKRMKGFCLIPQQSINEAIR [Numbering for GluA1 is for mature peptide, excluding 18 amino acid long signal peptide, following convention in the field.]
Human GluN2B (residues 1289-1310): KAQKKNRNKLRRQHSYDTFVDL
Human GluN2B(S1303D) (residues 1289-1310): KAQKKNRNKLRRQHDYDTFVDL
Human Densin-180 (residues 797-818): SKSRSTSSHGRRPLIRQDRIVG
Mouse Tiam1 (residues 1541-1559): RTLDSHASRMTQLKKQAAL

Full length peptide sequences for fluorescence polarization assays are as follows:
Human GluA1 (residues 813-837): KSRSESKRMKGFCLIPQQSINEAIR
Human GluN2B (residues 1289-1310): KAQKKNRNKLRRQHSYDTFVDL
Human GluN2B(S1303D) (residues 1289-1310): KAQKKNRNKLRRQHDYDTFVDL
Human Densin-180 (797-818): SKSRSTSSHGRRPLIRQDRIVG
Human CaMK2N1 (residues 37-58): GAGQNKRPPKLGQIGRSKRVVI
Mouse Tiam1 (residues 1541-1559): RTLDSHASRMTQLKKQAAL
Extended Syntide-2: GRRPLARTLSVAGLPGKK

508 **Crystallization and X-Ray Data Collection**
509 Initial crystallization screening was done using the sitting vapor diffusion method at 4°C with
510 commercially available screening kits. Initial hits were optimized by the hanging vapor diffusion
511 method if needed. Conditions yielded the crystal formation were included in Table S1, S2. The
512 ligand-to-protein ratio was kept at 3:1 throughout the co-crystallization attempts. Diffraction data
513 were collected from crystals flash-frozen in liquid nitrogen at a wavelength of 1.5418 Å using a
514 Rigaku MicroMax-007 HF X-ray source, which was coupled to a Rigaku VariMax HF optic
515 system (UMass Amherst). The X-ray data was collected at 100 K.
516
517 **Data Processing and Structure Determination**
518 Data sets were integrated, merged, and scaled using HKL-2000. The structures were solved by
519 molecular replacement (MR) with Phaser using the coordinates of CaMKIIα kinase domain
520 (PDB ID: 6VZK, 100% amino acid sequence identity) as a search model [39]. Peptides were
521 built into electron density using Coot and refinement was performed with REFMAC5 [40, 41].
522
523 **Fluorescence polarization assays**
524 Fluorescent polarization measurements were executed by adding 10 µL of 120 nM fluorescein-
525 labeled peptides (dissolved in 25 mM Tris pH 7.5, 150 mM KCl, 0.02% Tween, 0.02% Triton) to
526 10 µL of mutant CaMKII kinase domains at varying concentrations (25 mM Tris pH 7.5, 150 mM
527 KCl, 1 mM TCEP, 10% glycerol) in Corning low volume 384-well black flat bottom 384-well
528 plates. The concentration of ATP and $MgCl_2$ in peptide stock solution were adjusted to 500 µM
529 and 10 mM, respectively. The competition assay was conducted by mixing 10 µL of 2 µM
530 CaMKII kinase domain with 120 nM fluorescein-labeled GluN2B peptide with 10 µL of unlabeled
531 peptides at varying concentrations. The fluorescence polarization was measured using a
532 Synergy H1 hybrid plate reader (Biotek) with a filter of 485/20 nm excitation and 528/20 nm
533 emission. Data then was normalized by subtracting the background value ([protein] is zero)
534 from all data points and each value in the datasets was divided by the difference between the
535 highest concentration and zero concentration. All data were normalized to the corresponding
536 wild type measurement where the WT maximum FP value is set to 1. Data were fit using One
537 site- Specific binding with Hill slope in GraphPad PRISM version 6.01 after subtracting the
538 background value from individual values.
539
540 **Isothermal titration calorimetry**
541 ITC data were obtained using a MicroCal PEAQ-ITC automated calorimeter (Malvern
542 Panalytical, Westborough, MA). Before each titration, interaction partners were dissolved in gel
543 filtration buffer and final buffer conditions of CaMKII kinase domain and interaction partners
544 were matched. GluN2B peptides and CaMKIIN2 protein contain a single tyrosine residue, which
545 enabled accurate concentration determination. The other peptides lack aromatic residues, and
546 these required crude weight to estimate concentration. Titrations were performed with different
547 peptides as titrant into the cell containing D135N or other mutant CaMKII kinase domains
548 (concentrations are indicated in Table 3). All titrations were performed using the standard 19
549 injection method, modified to run at 20 °C. The standard 19 injection method in the PEAQ ITC
550 automated control software (v1.40) is one injection of 0.4 µL followed by 18 2 µL injections with
551 a spacing between injections of 150s, a stir speed of 750 rpm, and the reference power set to
552 10. Data were analyzed using PEAQ ITC analysis software (v1.40) using the one-site fitting
553 model, and to eliminate integration of some baseline noise, some integration markers were set
554 manually to obtain better fit.
555
556 **Differential scanning calorimetry**
557 Except where noted, all protein samples were diluted to 0.5 mg/mL in DSC buffer (25 mM Tris
558 pH 8,150 mM KCl, 1 mM TCEP, 10% glycerol). DSC measurements were performed on a

559 MicroCal Automated PEAQ-DSC instrument (Malvern Panalytical, Westborough, MA). Unless
560 otherwise indicated, after a 5 min pre-scan equilibration step, samples were scanned from 10-
561 120°C at a scan rate of 90°C/hr with no feedback. Data were analyzed using MicroCal PEAQ-
562 DSC software, and baseline-subtracted data were fit to a non-two-state fitting model to obtain
563 apparent T_m values.
564
565 **Molecular Dynamics simulations**
566 Trajectories were run for 1.2 μs - 3.7 μs aggregate time for each complex. Starting
567 conformations were taken from co-crystal structures of CaMKIIα kinase domain in complex with
568 peptides derived from GluN2B (PDB:6XBX) and Tiam1 (PDB:6XF0). For CaMKIIN1, Coot [41]
569 was used to superimpose the structure of a peptide derived from rat CaMKIIN1 in complex with
570 the kinase domain from *C. elegans* CaMKII (PDB:3KL8) with the structure of GluN2B in complex
571 with the kinase domain of CaMKIIα bound to a Mg^{2+} ion and an ATP molecule (PDB:6XBX). The
572 CaMKIIN1 peptide and the CaMKIIα kinase domain were then merged into a single structure.
573 Crystallographically unresolved atoms were added, peptides were extended in both N-terminal
574 and C-terminal directions, and E236K mutant versions of GluN2B and Tiam1 systems were
575 created using PDBFixer, part of the OpenMM package [42].
576
577 All simulations were performed with Gromacs 2020.2 [43, 44] and the CHARMM36m force field
578 [44]. Protein complexes were solvated with TIP3P water [45] in dodecahedral boxes that
579 extended 1 nm past the protein in all dimensions. Na^+ ions were added in sufficient quantity to
580 charge neutralize each system. Systems were energy-minimized by steepest descent for 50,000
581 steps using a 0.01 nm step size until the maximum force exerted on any atom fell below 1000
582 kJ/mol/nm. Solvent was equilibrated for 1 ns at constant temperature and volume (NVT
583 ensemble) and another 2 ns at constant temperature and pressure (NPT ensemble) with a
584 positional restraint applied to protein heavy atoms. Periodic boundary conditions were used in
585 all dimensions, bonds were constrained with the LINCS algorithm [46], virtual sites (v-sites)
586 were used to remove the fastest degrees of freedom to facilitate a 4 fs time step [47], particle
587 mesh Ewald (PME) was used to treat electrostatic interactions [48], the v-rescale thermostat
588 [49] with a 0.1 ps coupling time constant was used to maintain the temperature at 300 K, and a
589 cut-off distance of 1.2 nm for neighbor list, Coulomb interactions, and Van der Waals
590 interactions was used throughout system preparation and production simulations. The
591 Parrinello–Rahman barostat [50] with a 2 ps coupling time constant was used to maintain a
592 pressure of 1 bar during NPT equilibration and production simulations. V-site parameters for
593 ATP were determined using MkVsites [51].
594
595 One production simulation was performed for each of the wild type kinase:GluN2B and wild type
596 kinase:Tiam1 complexes, producing trajectories of 2.19 μs and 2.05 μs, respectively. Two
597 independent simulations were performed for each of wild type kinase:CaMKIIN1 and E236K
598 kinase:GluN2B complexes. The CaMKIIN1 trajectories were 0.46 μs and 1.84 μs in length, for
599 an aggregate of 2.3 μs. The GluN2B trajectories were 0.68 μs and 0.57 μs in length, for an
600 aggregate of 1.25 μs. Four independent simulations were performed for the E236K
601 kinase:Tiam1 complex, producing trajectories of 1.66 μs, 1.23 μs, 1.02 μs, and 0.77 μs, for an
602 aggregate of 4.68 μs. Trajectories were analyzed using MDTraj [52].
603
604 **Coupled kinase assays**
605 Kinase activity was monitored using a Synergy H1 microplate reader (Biotek) as previously
606 described [20, 53]. The assay was conducted in 50 mM Tris, 150 mM KCl, 10 mM $MgCl_2$, 2 mM
607 ATP, 1 mM Phosphoenolpyruvate (Alfa Aesar), 0.2 mM Nicotinamide adenine dinucleotide
608 (Sigma), 10 units/mL Pyruvate kinase (Sigma), 30 units/mL Lactate dehydrogenase (Millipore

609 Sigma), varying concentrations of Syntide-2 (Lifetein). The final CaMKII kinase domain
610 concentration was 5 nM. 500 nM CaMKIIN2 protein or 8.14 μM NMDAR(S1303D) peptide was
611 preincubated with CaMKII kinase domain before adding to the reaction mix of corresponding
612 experiments. The reactions were started by the addition of ATP to the reaction mix and the
613 absorbance was measured at 340 nM at 30°C at 10 and 15 sec intervals for 10 minutes. The
614 rate was obtained by calculating the maximum observed slope of each reaction. Data were fit
615 using the Michaelis-Menten equation in GraphPad PRISM version 6.01.
616
617 **Immunoprecipitation**
618 HEK293T cell lysates were prepared in lysis buffer (50 mM Tris-HCl pH 7.5, 150 mM NaCl, 1%
619 Triton X-100, 10% glycerol, 1 mM Na_3VO_4, 10 mM NaF, 1 mM β-glycerophosphate, 1 x
620 phosphatase inhibitor cocktail (Nacalai, Kyoto, Japan), 1x complete tablet (Roche, Basel,
621 Switzerland) and centrifuged at 14,000 rpm for 10 min at 4°C. The supernatant was subjected to
622 immunoprecipitation using 20 μL of the anti-Flag antibody-beads (Sigma) for 2-4 hours at 4°C.
623 Beads were washed with 1 mL of lysis buffer for three times. Bound proteins were eluted with
624 SDS-PAGE sample buffer and subjected to western blotting.
625
626 **Data availability**
627 Atomic structures have been deposited in the PDB, listed in the table below.
628
629 Table of PDB codes and descriptions.
630

6X5G	Inactive kinase in complex with Densin-180
6X5Q	Inactive kinase in complex with GluA1
6X8V	Inactive kinase in complex with Tiam1
6XF0	Inactive kinase in complex with Tiam1 and ATP
6XBP	Inactive kinase in complex with GluN2B and Hecameg
6XBX	Inactive kinase in complex with GluN2B and ATP
6XDL	Active kinase in complex with GluN2B
6XDU	Active kinase in complex with GluN2B and ADP
7KL0	Inactive kinase in complex with phosphomimetic GluN2B and Hecameg
7KL1	Inactive kinase in complex with phosphomimetic GluN2B and ATP
7KL4	Inactive kinase in complex with phosphomimetic GluN2B
6XOE	Inactive kinase in complex with phosphomimetic GluN2B and ATP
7KL2	Inactive kinase in complex with phosphomimetic GluN2B

631

632 **ACKNOWLEDGMENTS**

633 We thank Roger Colbran for helpful discussions. This work was supported by start-up funds
634 from UMass Amherst (M.S.), SPIRITS 2019 of Kyoto University, Grant-in-Aid for Scientific
635 Research 18H04733, and 18H05434 from the MEXT, Japan and HFSP Research Grant
636 (RGP0020/2019) (Y.H.).

637
638 Conflict of interest: YH received research funds from Fujitsu Laboratories and Dwango.

639 **Author Contributions**
640 C.Ö. solved all crystal structures and performed all FP measurements and kinetic assays. T.M.
641 and T.S. performed immunoprecipitation experiments. N.S., E.A., C.G., E.L., J.F. and E.A.E.
642 also assisted with experiments under supervision of B.A.K., S.C.G., Y.H. and M.M.S. R.S.

643 performed molecular dynamics. C.Ö., R.S., Y.H., B.A.K., and M.M.S. wrote and edited the
644 manuscript.
645
646
647 **FIGURES**

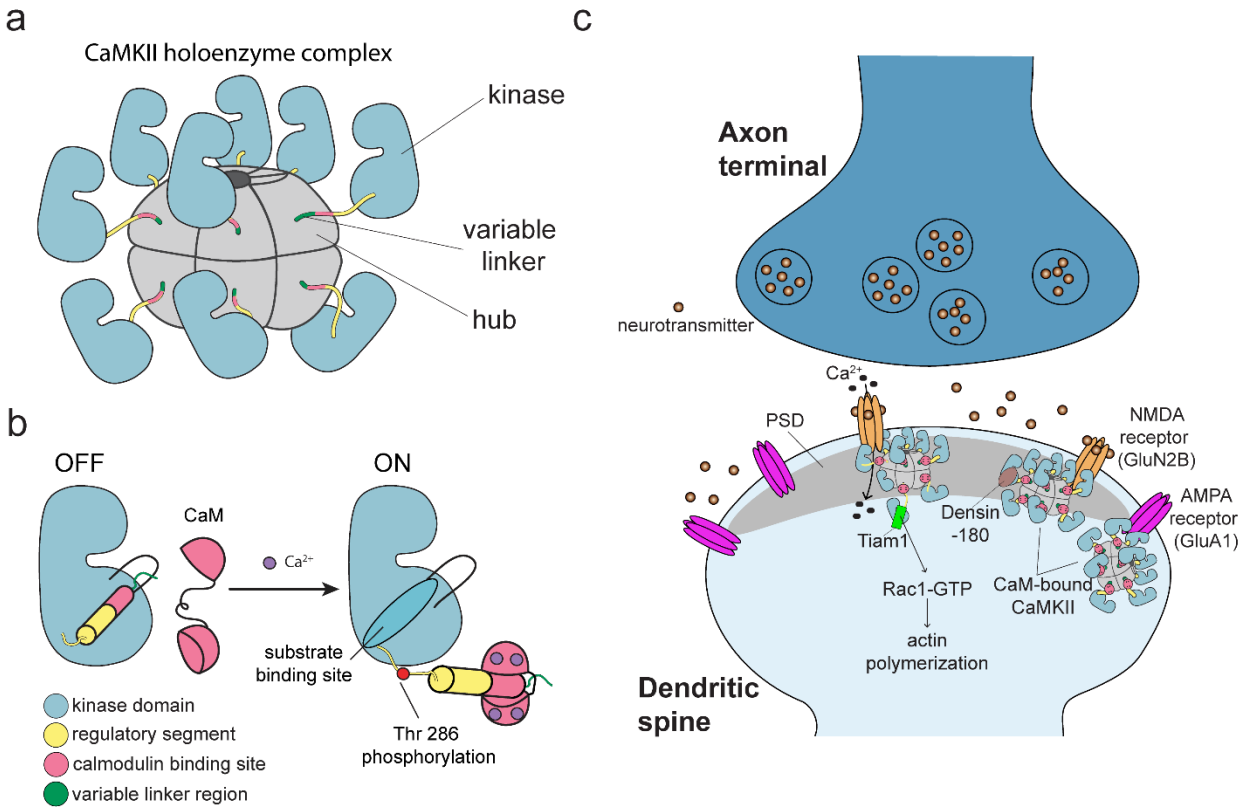

648
649
650 **Figure 1. CaMKII architecture and the interaction partners at excitatory synapses**
651 (a) The architecture of a dodecameric CaMKII holoenzyme. (b) Ca^{2+}/CaM binding activates
652 CaMKII by competitively binding the regulatory segment thereby freeing the substrate binding
653 site. Active CaMKII autophosphorylates at Thr 286. (c) CaMKII interactions at the excitatory
654 postsynaptic structure, mostly in the post synaptic density (PSD) of the denritic spine.
655
656

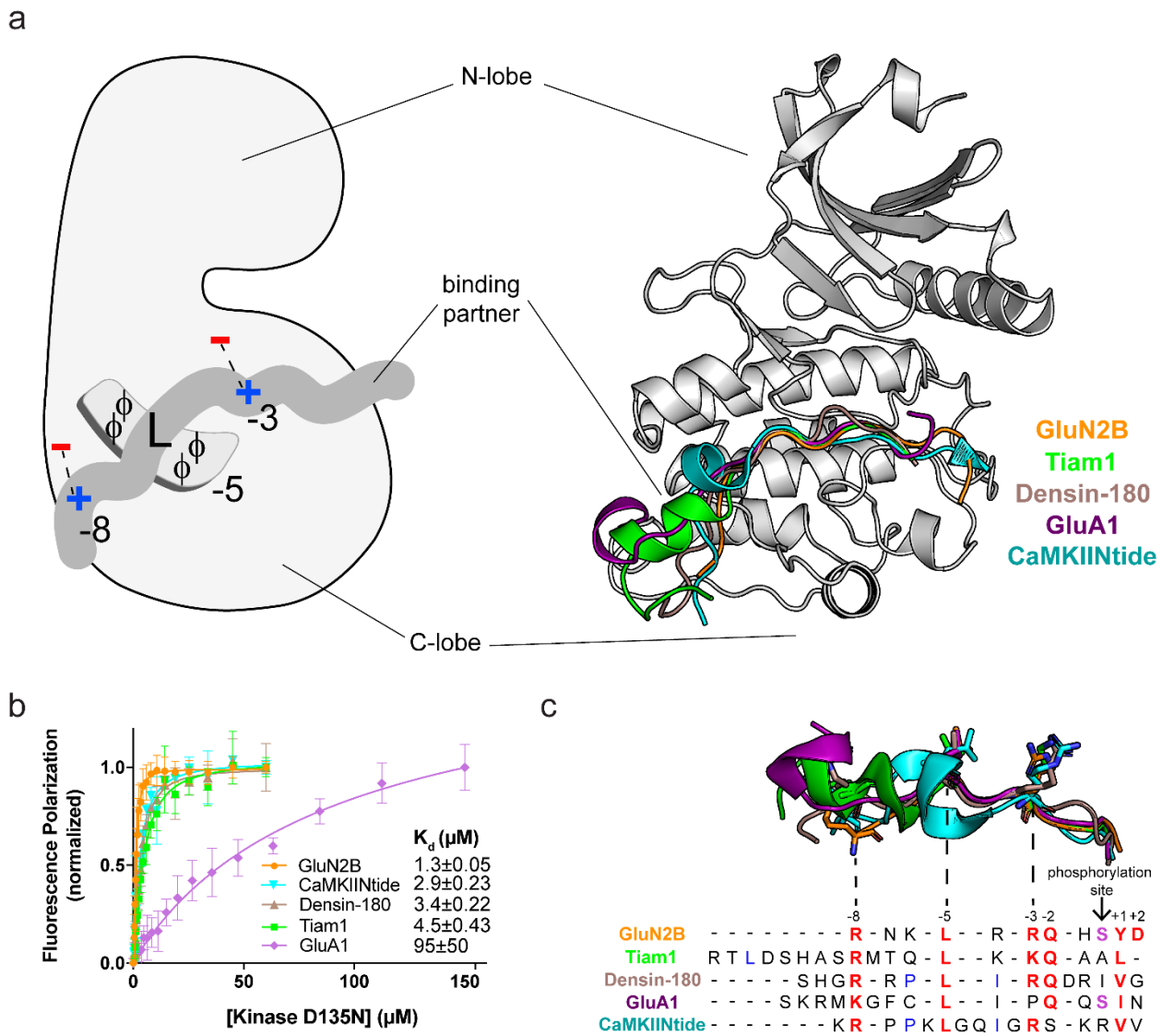

Figure 2. CaMKII kinase domain interactions with the binding partners. (a) Left: Schematic diagram of the interactions with binding partners. Phi symbol indicates hydrophobic residues. Green symbols indicate those identified from molecular dynamics simulations. Right: overlay of five cocrystal structures, peptides shown as cartoon in corresponding colors in (a). (b) Binding measurements for GluN2B, Tiam1, Densin-180, CaMKIINtide, and GluA1 using fluorescence polarization. (c) The sequence alignment of CaMKII binding partners. Aligned peptide structures are above. Conserved residues highlighted in red. Phosphosite residues on substrates are highlighted in purple. Residues involved in a docking event with W214 are highlighted in blue.

667

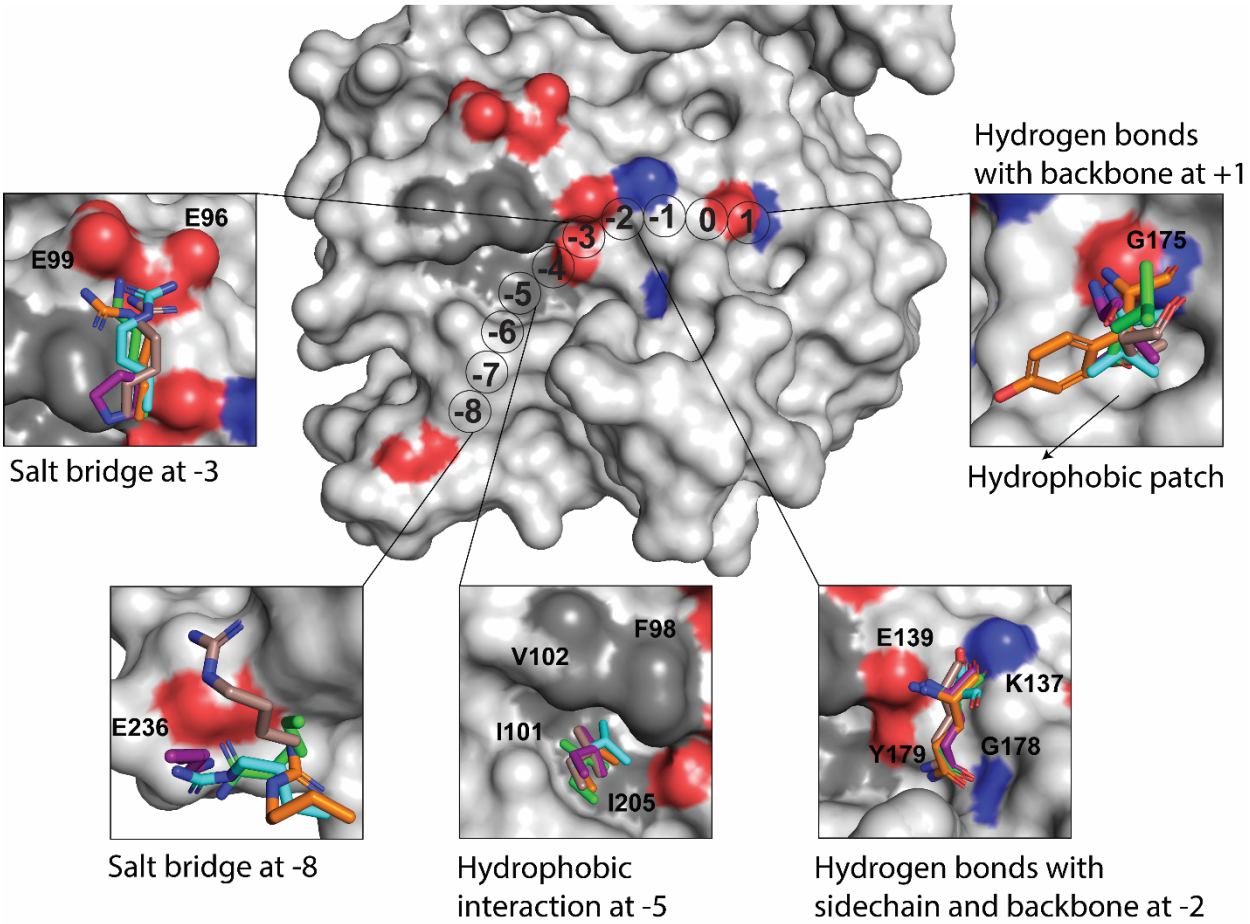

668
669 **Figure 3. Conserved binding motifs on the catalytic domain surface.**
670 Surface representation of the CaMKII kinase domain highlighting residues shown to interact with
671 binding partners.
672

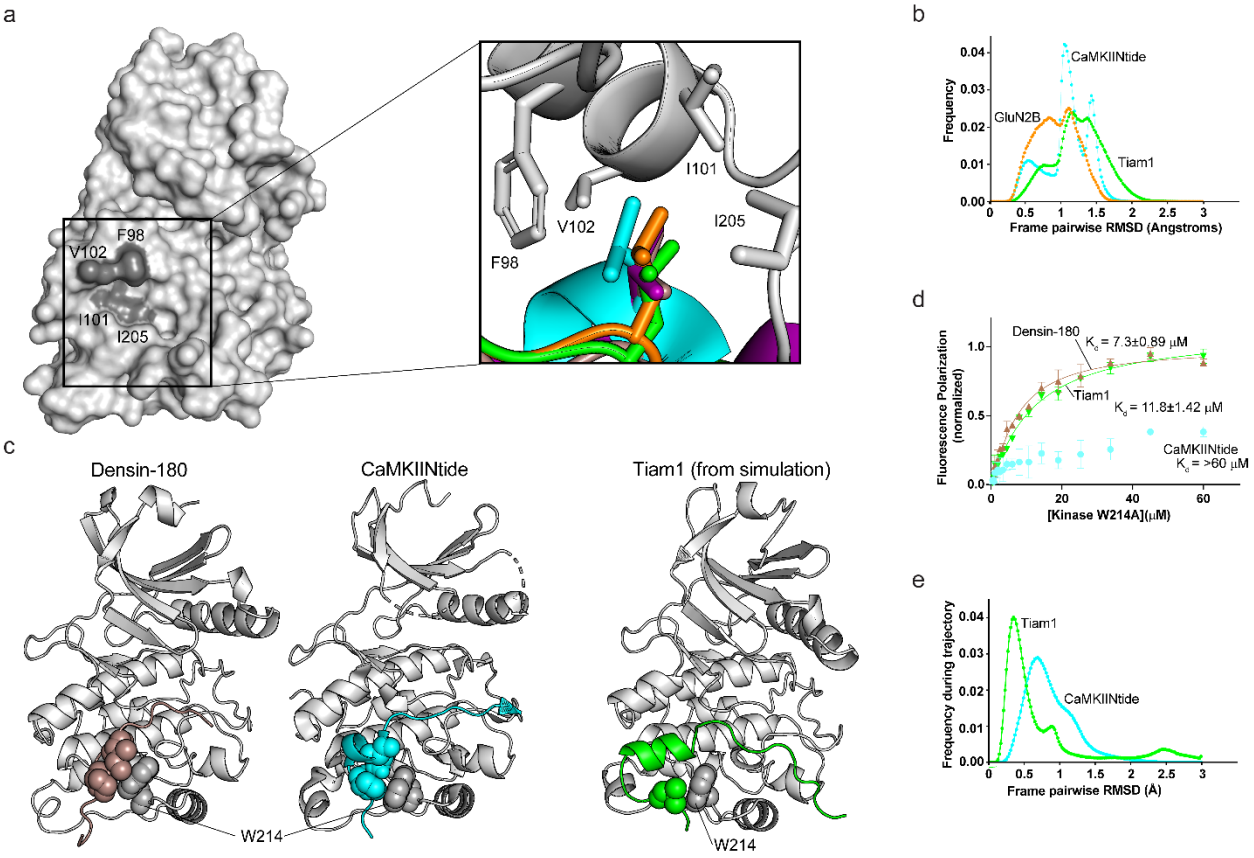

Figure 4. Hydrophobic interactions mediate binding. (a) Surface representation of CaMKII kinase domain with residues forming the hydrophobic pocket labeled. Zoom in: Overlay of leucine residues from all co-crystal structures bound in the hydrophobic pocket. (b) Histograms of RMSD between every pair of trajectory frames for F98, I101, V102, and I205 with -5 peptide leucine. (c) Sphere representation of the isoleucine and proline or leucine residue of Densin-180 (brown), CaMKIIN (cyan), and Tiam1 (green) docking onto W214 (gray) of kinase domain. (d) FP measurements of the CaMKII kinase domain with W214A mutation binding to CaMKIIN (cyan), Densin-180 (brown), and Tiam1 (green) peptides. (e) RMSD histograms for W214 interacting with isoleucine and proline of CaMKIIN1 and leucine of Tiam1 as seen in 3c.

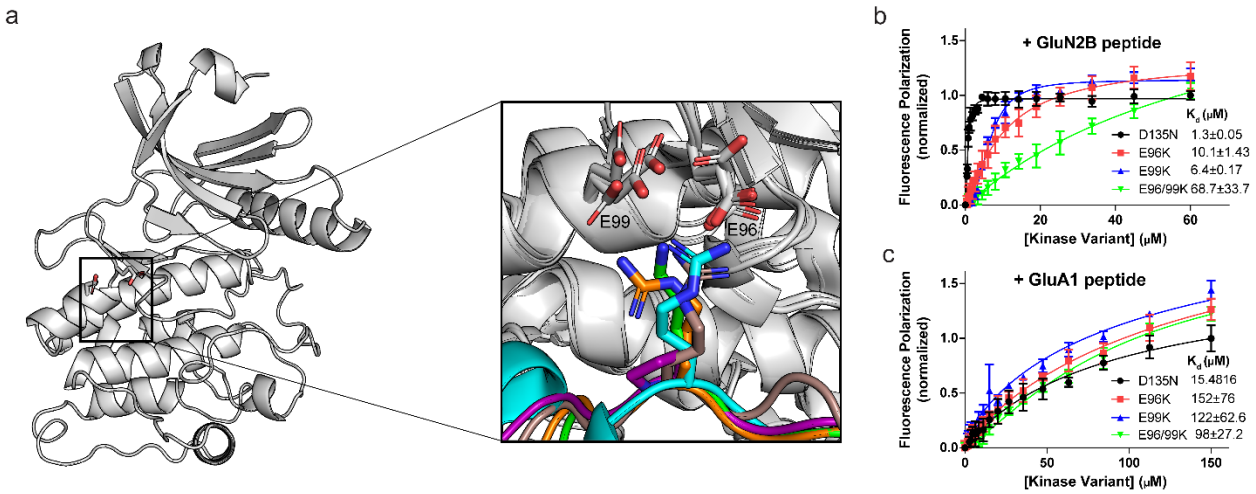

Figure 5. Electrostatic interactions with E96 and E99 facilitate high affinity binding. (a) CaMKII kinase domain shown as a cartoon, E96 and E99 residues are shown in sticks. Inset: zoom in of all five co-crystal structures overlaid. (b) FP measurements of the CaMKII kinase domain with E96K (red), E99K (blue), and E9699K (green) mutations binding to the GluN2B peptide and (c) to the GluA1 peptide.

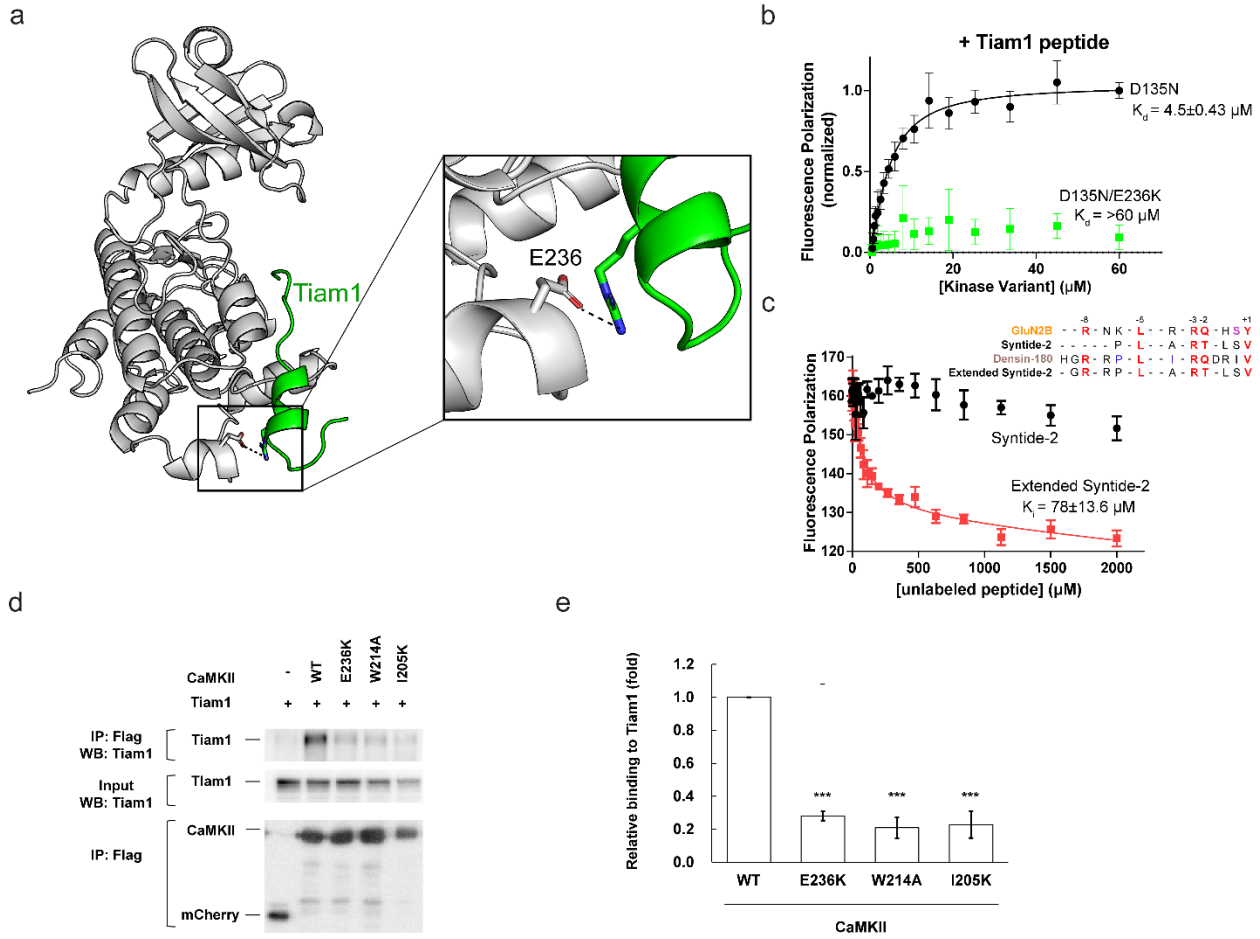

Figure 6. Electrostatic interaction with E236 has distinctive effects on binding. (a) View of the interaction between CaMKII E236 residue (gray) and Tiam1 R1549 residue (green). (b) FP measurements of the CaMKII kinase domain with E236K mutation binding Tiam1 (green) peptide. (c) Competition assay against GluN2B using Syntide-2 (black) and extended version of Syntide-2 (red). (d, e) Effects of CaMKII mutations (E236K, W214A and I205K) on interaction with Tiam1. HEK293T cells were co-transfected with Flag-tagged CaMKII variants and Tiam1-mGFP. Cell lysates were immunoprecipitated with Flag antibody, and samples were immunoblotted with Tiam1 and Flag antibodies. (d) Representative blots. (e) Quantification of the co-immunoprecipitated Tiam1 with CaMKII from 3 independent experiments. The amount of co-immunoprecipitated Tiam1-mGFP was normalized by the amount in cell lysate and immunoprecipitated CaMKII. ***$p < 0.01$, compared to WT CaMKII (n=3); one-way ANOVA with the Shaffer's post hoc test comparisons. WT, wild type; IP, immunoprecipitation.

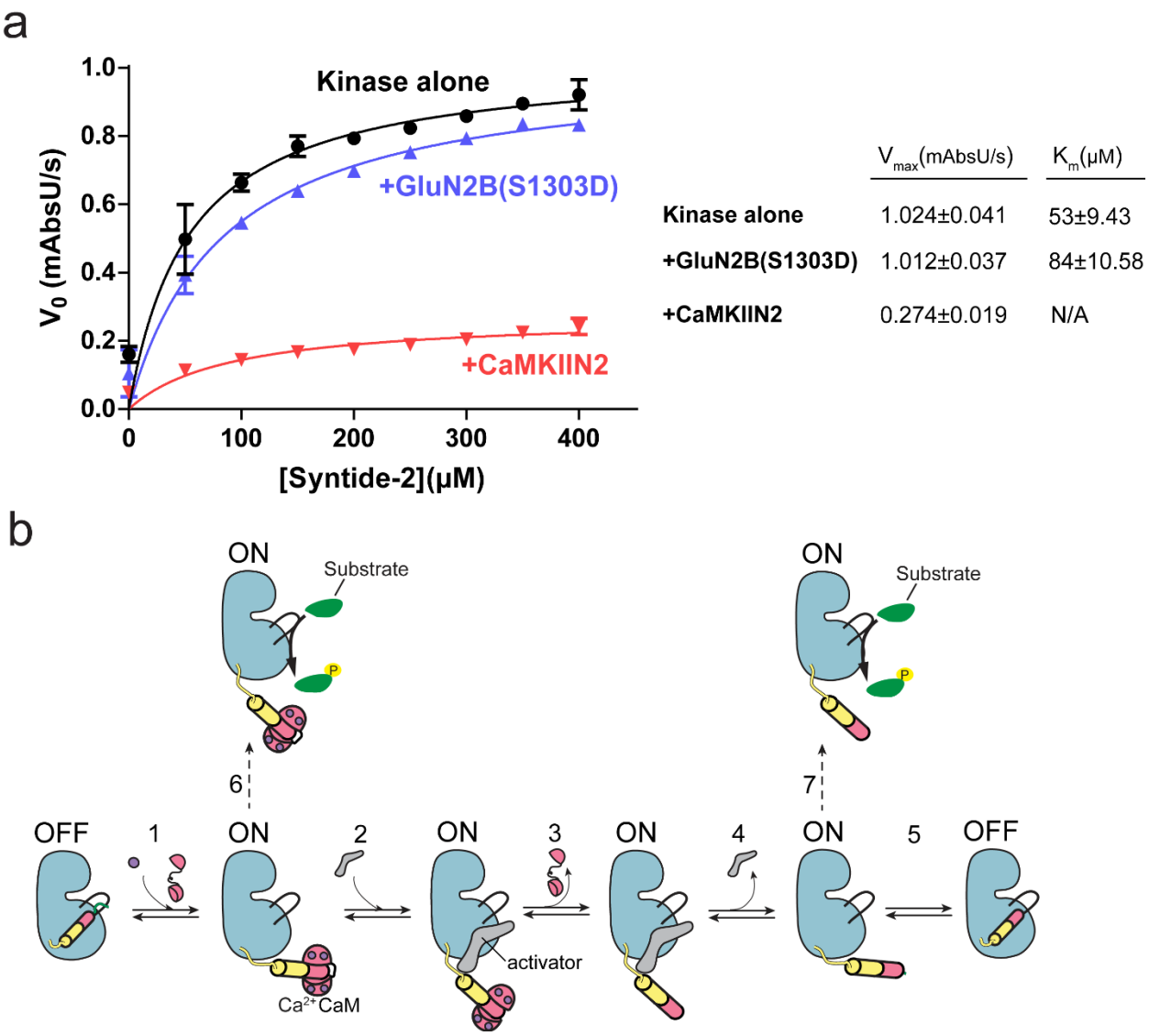

Figure 7. GluN2B acts as a competitive inhibitor on CaMKII (a) Coupled kinase assay results with kinase alone, in the presence of GluN2B and CaMKIIN2. (b) Proposed model of maintaining CaMKII activity by binding to a high affinity activator. CaMKII binds Ca^{2+}/CaM and is activated (Rxn 1). Phosphorylation of substrates occurs in this state (Rxn 6). A high affinity activator binds to the substrate binding site (Rxn 2). When the Ca^{2+} signal dissipates, CaM dissociates from CaMKII, but the activator remains bound, competing with the regulatory segment (Rxn 3). The activator dissociates (Rxn 4), allowing another substrate to bind and be phosphorylated (Rxn 7) before either the regulatory segment rebinds (Rxn 5) or the activator rebinds (Rxn 4).

Tables. Data Collection and Refinement Statistics

Table 1. GluN2B WT and S1303D cocrystal structures

	GluN2B+ADP(active kinase) (6XDU)	GluN2B(active kinase) (6XDL)	GluN2B+ATP (6XBX)	GluN2B-Hecameg (6XBP)	GluN2B(S1303D)+ATP (7KL1)	GluN2B(S1303D)-ATP (6XOE)	GluN2B(S1303D) (PDB 7KL4)	GluN2B(S1303D) (PDB 7KL2)	GluN2B(S1303D)+Hecameg (7KL0)
Crystallization conditions	0.1 M Bis-tris propane pH 6.6, 0.1 M Ammonium sulfate, 20% PEG 3350,	0.1 M Bis-tris propane pH 6.2, 0.1 M Ammonium sulfate, 20% PEG 3350, 5% Ethanol	0.1 M Bis-tris methane pH 6.2, 0.1 M Ammonium sulfate, 25% PEG 3350, 19mM Methyl 6-O-(N-heptylcarbamoyl)-alpha-D-glucopyranoside	0.1 M Bis-tris methane pH 6.2, 0.1 M Ammonium sulfate, 25% PEG 3350, 19mM Methyl 6-O-(N-heptylcarbamoyl)-alpha-D-glucopyranoside	0.1 M Bis-tris methane pH 6.5, 0.1 M Ammonium sulfate, 20% PEG 6000, 19mM Methyl 6-O-(N-heptylcarbamoyl)-alpha-D-glucopyranoside	0.1 M Bis-tris propane pH 6.5, 0.2 M Sodium chloride, 25% PEG 3350	0.1 M Bis-tris propane pH 6.5, 0.2 M Sodium chloride, 25% PEG 3350	0.15 M DL-Malic acid pH 7, 20% PEG 3350	0.1 M Bis-tris methane pH 6.5, 0.1 M Ammonium sulfate, 20% PEG 6000, 19mM Methyl 6-O-(N-heptylcarbamoyl)-alpha-D-glucopyranoside
Data collection									
Space group	$P12_11$	$P12_11$	$P2_12_12_1$	$P2_12_12_1$	$P2_12_12_1$	$P12_11$	$P12_11$	$P12_11$	$P2_12_12_1$
Cell dimensions									
a, b, c (Å)	45.01, 65.23, 53.71	45.09, 66, 45	73.14, 91.42, 91.92	73.25, 91.78, 91.77	72.89, 92.13, 91.34	47.31, 67.25, 45.72	43.40, 71.42, 45.27	44.78, 65.16, 54.1	72.99, 91.29, 92.08
α, β, γ (°)	90, 95.26, 90	90, 97.61, 90	90, 90, 90	90, 90, 90	90, 90, 90	90, 94.43, 90	90, 97.48.8, 90	90, 95.8, 90	90, 90, 90
Resolution (Å)	50 – 2.75 (2.85 – 2.8)	50 – 1.95 (1.99 – 1.96)	50 – 2.56 (2.60 – 2.56)	50 – 2.25 (2.29 – 2.25)	50 – 2.4 (2.44 – 2.4)	50 – 2.1 (2.14 – 2.1)	50 – 2.24 (2.29 – 2.25)	50 – 2.55 (2.59 – 2.55)	50-2.4 (2.44-2.4)
R_{merge}	0.102 (0.374)	0.13 (0.485)	0.232 (0.812)	0.116 (0.374)	0.183 (0.527)	0.098 (0.297)	0.198 (1.671)	0.199 (0.776)	0.188 (0.627)
Mean $I/\sigma I$	5 (1.57)	9.5 (2)	5 (1.86)	9.3 (4.36)	5.9 (2.65)	9.9 (3.51)	4.2 (0.524)	3.2 (0.44)	4.9 (2.04)
Completeness (%)	93.8 (90.9)	93.8 (82.7)	100 (99.8)	96.9 (90.1)	99.9 (98.8)	99.6 (97.3)	94.5 (75.5)	99.5 (97.7)	99.9 (99.5)
Redundancy	2.6 (2.5)	2.7 (2.5)	6.3 (5.4)	6.3 (5.7)	5.7 (5)	3.3 (2.8)	3.3 (2.8)	3.1 (2.6)	5.6 (4.9)
$CC_{1/2}$	0.985 (0.711)	0.956 (0.678)	0.976 (0.572)	0.99 (0.868)	0.976 (0.740)	0.993 (0.824)	0.979 (0.169)	0.975 (0.255)	0.984 (0.652)
CC*	0.996 (0.912)	0.989 (0.899)	0.994 (0.853)	0.997 (0.964)	0.994 (0.922)	0.998 (0.951)	0.995 (0.538)	0.994 (0.638)	0.996 (0.888)
Refinement									
Resolution (Å)	44.86 – 2.8 (2.824 – 2.753)	33.92 – 1.96 (2.002 – 1.951)	48.56 – 2.56 (2.626 – 2.56)	45.93 – 2.25 (2.31 – 2.252)	48.5 – 2.4 (2.46 – 2.4)	38.65 – 2.1 (2.154 – 2.1)	30.2 – 2.25 (2.296 – 2.25)	41.53 – 2.56 (2.623 – 2.56)	48.52 – 2.4 (2.46 – 2.4)
Unique reflections	7103 (428)	16929 (1027)	19465 (1411)	27648 (1847)	23497 (1650)	15852 (1096)	11903 (714)	9458 (577)	23396 (1610)
R_{work} / R_{free}	17.9%/26.75%	18.41%/24.63%	20.33%/28.75%	18.83%/25.91%	19.01%/26.48%	17.82%/24.3%	21.87%/ 30.05%	24.17%/ 29.29%	19.17%/25.73%
No. atoms									
Protein	2235	2234	4479	4507	4518	2268	2243	2243	4497
Water	27	89	60	168	163	115	16	16	194
Ligand	31	35	82	64	108	44			94
B-factors									
Protein	39.05	31.23	32.11	28.04	28.16	28.73	49.80	49.80	26.25
Water	23.83	33.77	19.31	23.02	23.29	29.96	25.26	25.26	22.19
Ligand	74.28	45.19	50.76	26.47	34.43	41.75			34.51
R.m.s. deviations									
Bond lengths (Å)	0.0056	0.0085	0.0086	0.0083	0.0103	0.0081	0.0067	0.0049	0.0105
Bond angles (°)	1.4012	1.5357	1.6530	1.5758	1.6708	1.5531	1.4669	1.4676	1.7230

Table 2. Tiam1, Densin-180 and GluA1 cocrystals structures

	Tiam1+ATP (6XF0)	Tiam1 (6X8V)	Densin-180 (PDB 6X5G)	GluA1 (6X5Q)
Crystallization conditions	16% PEG 6K, 0.1 M HEPES pH 7, 0.1% Triton X 114	0.1 M HEPES pH 7, 16% PEG 6K, 0.1% Triton X 114	0.1 M Bicine pH 9, 10% PEG 20K, 2% 1,4 Dioxane	0.1 M Tris pH 8, 28% PEG 4K
Data collection				
Space group	$P2_12_12_1$	$P2_12_12_1$	$P12_11$	$P2_12_12_1$
Cell dimensions				
a, b, c (Å)	43.49, 138.84, 154.97	43.43, 137.41, 156.47	36.29, 66.17, 61.71	42.63, 57.46, 107.71
α, β, γ (°)	90, 90, 90	90, 90, 90	90, 99.78, 90	90, 90, 90
Resolution (Å)	50 – 2.71 (2.76 – 2.71)	50 – 2.560 (2.6 – 2.56)	33.11 - 1.85 (1.88-1.85)	50 – 2.1 (2.18 - 2.14)
R_{merge}	0.354 (2.294)	0.348 (2.359)	0.065 (0.325)	0.179 (0.377)
Mean $I/\sigma I$	3 (0.5)	2.8 (0.42)	9.6 (3.14)	3.2 (2.21)
Completeness (%)	96 (89.7)	92.2 (90.9)	93.6 (86.5)	96.9 (92.7)
Redundancy	5.1 (3.8)	3.9 (2.8)	3.4 (3.3)	4.9 (4.4)
$CC_{1/2}$	0.975 (0.146)	0.962 (0.011)	0.99 (0.829)	0.992 (0.82)
CC*	0.994 (0.504)	0.99 (0.149)	0.997 (0.952)	0.998 (0.949)
Refinement				
Resolution (Å)	41.91 – 2.71 (2.783 – 2.713)	48.81 – 2.56 (2.622 – 2.56)	33.11 - 1.85 (1.88-1.85)	39.32 – 2.14 (2.159 – 2.104)
Unique reflections	23988 (1554)	27363 (1837)	22043 (1067)	14475 (798)
R_{work} / R_{free}	22.86%/30.08%	26.03%/31%	18.65%/22.65%	18.93%/23.5%
No. atoms				
Protein	4461	4460	2259	2241
Water	83	30	111	96
Ligand	123	35	23	18
B-factors				
Protein	49.28	38.27	24.12	17.35
Water	24.5	11.57	25.6	14.48
Ligand	66.14	50.73	54.41	30.61
R.m.s. deviations				
Bond lengths (Å)	0.0077	0.0068	0.0095	0.0080
Bond angles (°)	1.5724	1.5884	1.6271	1.5184

743 **SUPPLEMENTAL FIGURES**

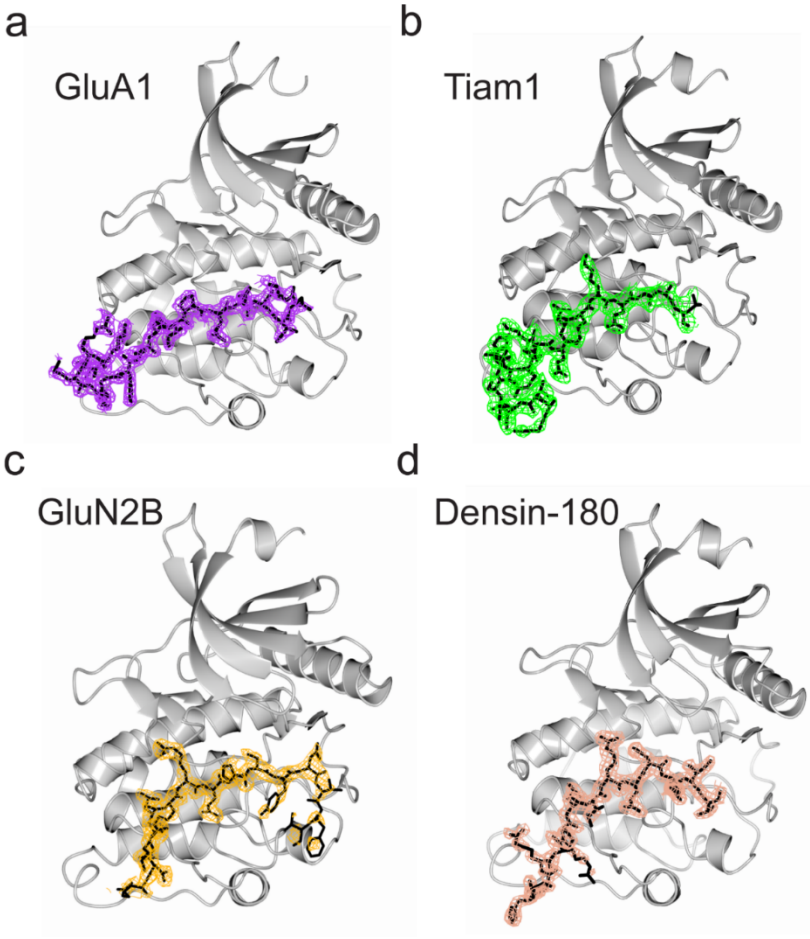

744
745
746 **Figure S1. Structures of CaMKII kinase domain bound to peptide binding partners.**
747 Electron density is shown for all peptide binding partners: (a) GluA1, (b) Tiam1, (c) GluN2B, and
748 (d) Densin-180.
749

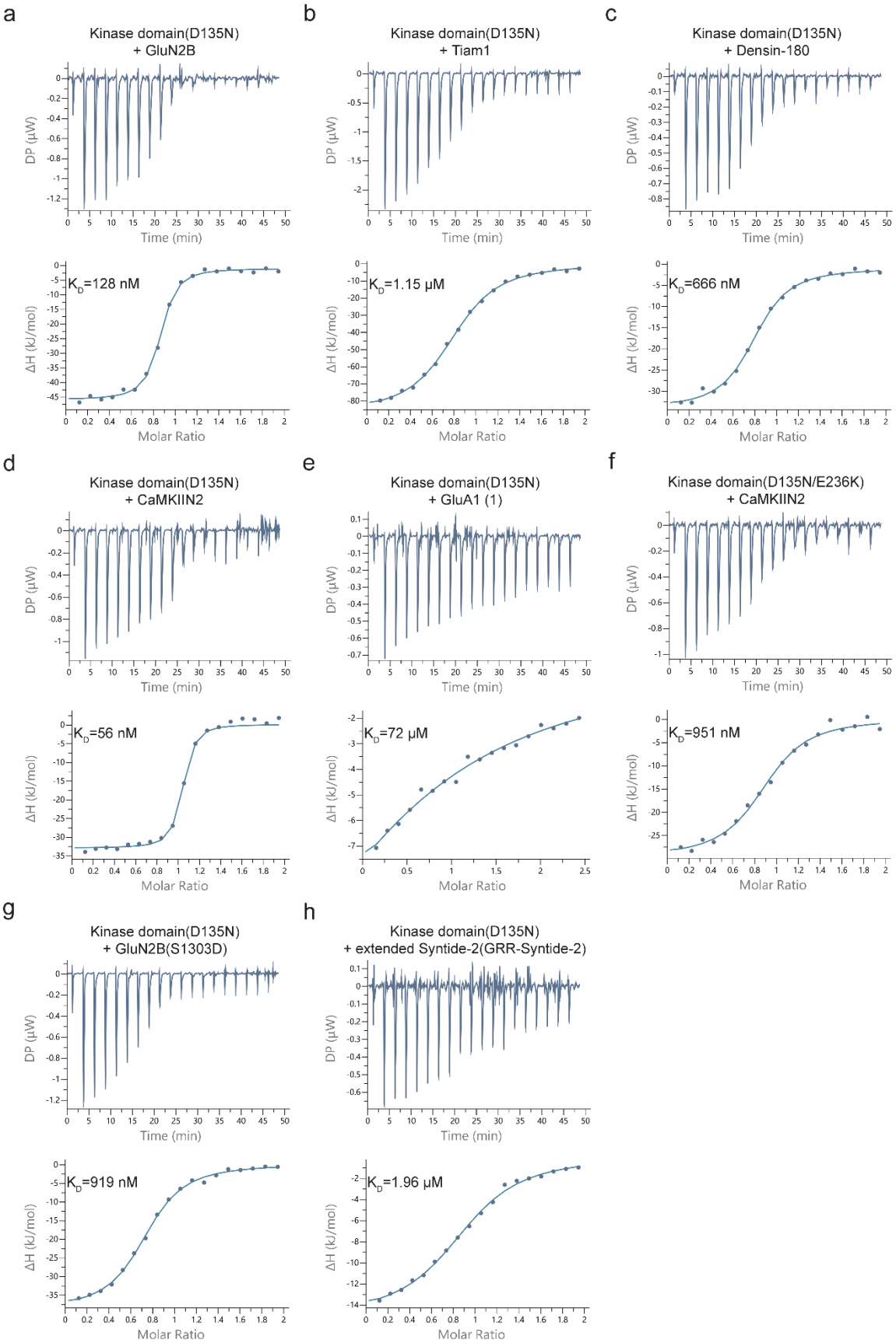
a
Kinase domain(D135N)
+ GluN2B
DP (μW)
Time (min)
ΔH (kJ/mol)
Molar Ratio
K_D=128 nM
b
Kinase domain(D135N)
+ Tiam1
K_D=1.15 μM
c
Kinase domain(D135N)
+ Densin-180
K_D=666 nM
d
Kinase domain(D135N)
+ CaMKIIN2
K_D=56 nM
e
Kinase domain(D135N)
+ GluA1 (1)
K_D=72 μM
f
Kinase domain(D135N/E236K)
+ CaMKIIN2
K_D=951 nM
g
Kinase domain(D135N)
+ GluN2B(S1303D)
K_D=919 nM
h
Kinase domain(D135N)
+ extended Syntide-2(GRR-Syntide-2)
K_D=1.96 μM

750

751 **Figure S2. ITC data show tighter binding to peptides in the absence of denaturant.**
752 Isothermal scanning calorimetry data from CaMKII kinase domain (D135N) binding to (a)
753 GluN2B peptide, (b) Tiam1 peptide, (c) Densin-180 peptide, (d) CaMKIIN2 protein, (e) GluA1
754 peptide. (f) CaMKIIN2 protein with additional E236K mutation on the CaMKII kinase, (g) GluN2B
755 (S1303D) peptide, and (h) extended Syntide-2 peptide.
756

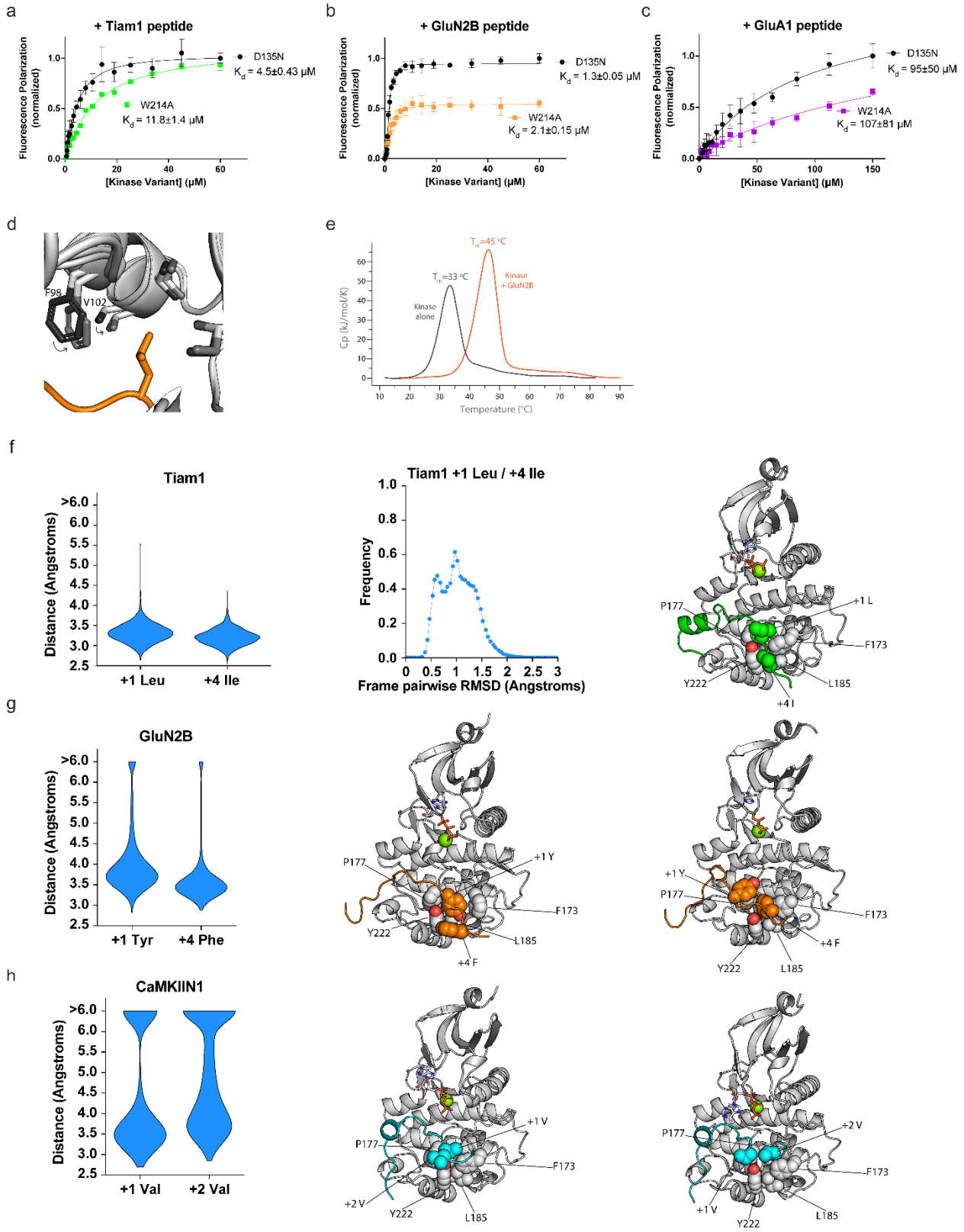

Figure S3. Three hydrophobic interaction sites mediate peptide binding. FP measurements of the CaMKII kinase domain with W214A mutation binding to (a) Tiam1 (green),

(b) GluN2B (orange), and (c) GluA1 (purple) peptides. (d) Overlay of CaMKII kinase domain alone (PDB 6VZK) shown in dark gray and CaMKII kinase domain-GluN2B structure (PDB 6XBP) shown in lighter gray. F98 and V102 of CaMKII kinase domain undergo spatial rearrangement upon leucine binding to the hydrophobic core. (e) Differential Scanning Calorimetry data from CaMKII kinase domain alone (brown) and CaMKII kinase domain bound to GluN2B peptide (orange). (f) Persistence of Tiam1 interaction with the F173, P177, L185, Y222 hydrophobic patch in MD simulations. Distance distributions for +1 leucine and +4 isoleucine of Tiam1 to patch (left), RMSD histogram for +1 leucine, +4 isoleucine, and the four residues that make up the patch (middle), representative structure (right). (g) Persistence of GluN2B interaction with hydrophobic patch. Distance distributions for +1 tyrosine and +4 phenylalanine of GluN2B and two representative structures. (h) Persistence of CaMKIIN1 interaction with hydrophobic patch. Distance distributions for +1 and +2 valine residues of CaMKIIN1 and two representative structures.

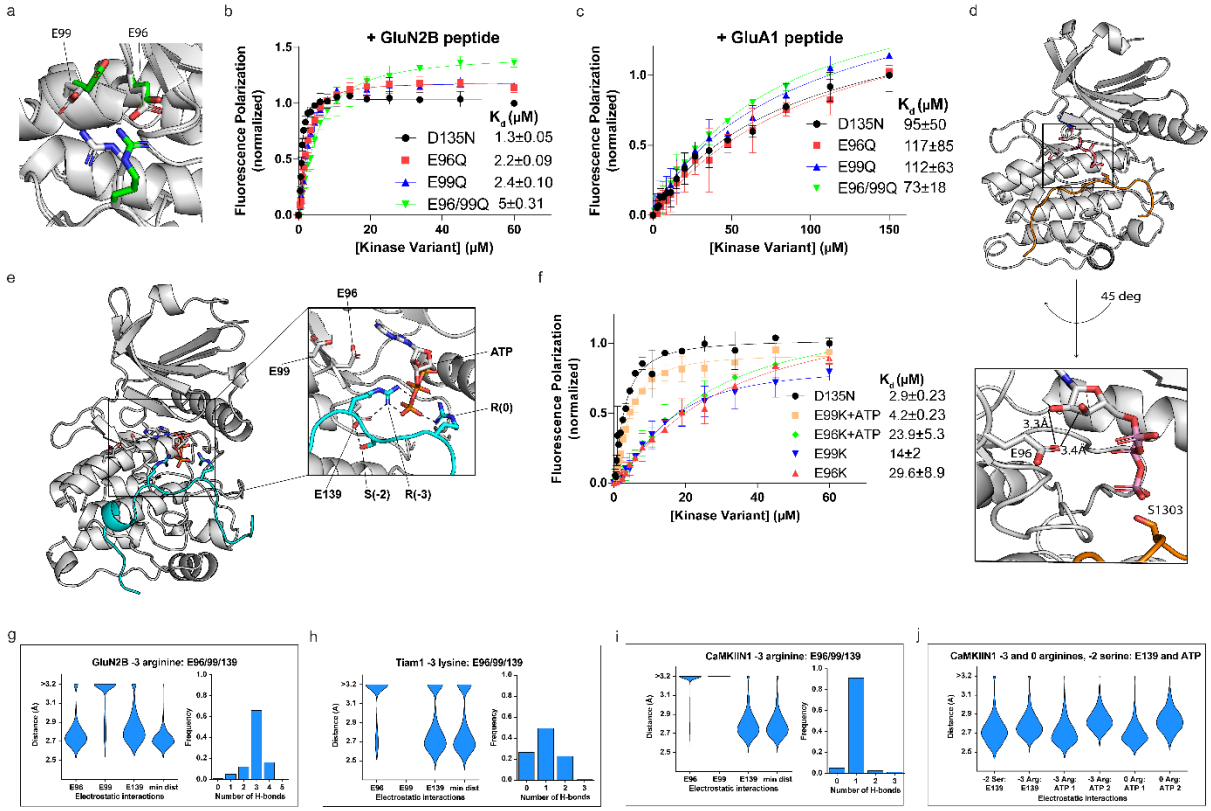

Figure S4. E96, E99, and E139 regulate peptide interactions and ATP binding. (a) R(-3) of GluN2B peptide is seen in different orientations relative to E96 and E99 of CaMKII kinase domain in separate crystal structures, 6XBP (light gray) and 6XDL (green). FP measurements of the CaMKII kinase domain with E96Q-E99Q-E96/99Q mutations binding to GluN2B (b) and GluA1 (c) peptides. (d) Co-crystal structure of CaMKII kinase domain and GluN2B in complex with ATP (PDB 6XBX). Phosphorus shown in pink. Bottom image highlights the interaction between E96 sidechain and ribose hydroxyl groups of ATP. (e) Snapshot from MD simulations with CaMKIIN1 peptide in the presence of ATP. All interaction depicted with dashed lines are below 3 Å. (f) FP measurements of CaMKII kinase domain with E96K-E99K mutations binding to CaMKIIN1 in the absence and presence of ATP. (g-i) Electrostatic interactions between -3 peptide residue and E96, E99, and E139 in MD simulations. Distance distributions for -3 residue to each glutamic acid side chain and shortest of the three distances (left) and histogram of the

number of H-bonds formed between the -3 residue and the three glutamic acid side chains (right) for the (g) -3 arginine of GluN2b, (h) -3 lysine of Tiam1, and (i) -3 arginine of CaMKIIN1. (j) Distance distributions for 0 arginine, -2 serine, and -3 arginine of CaMKIIN1 to E139 and and to ATP phosphates. 0 and -3 arginines each make two contacts with ATP.

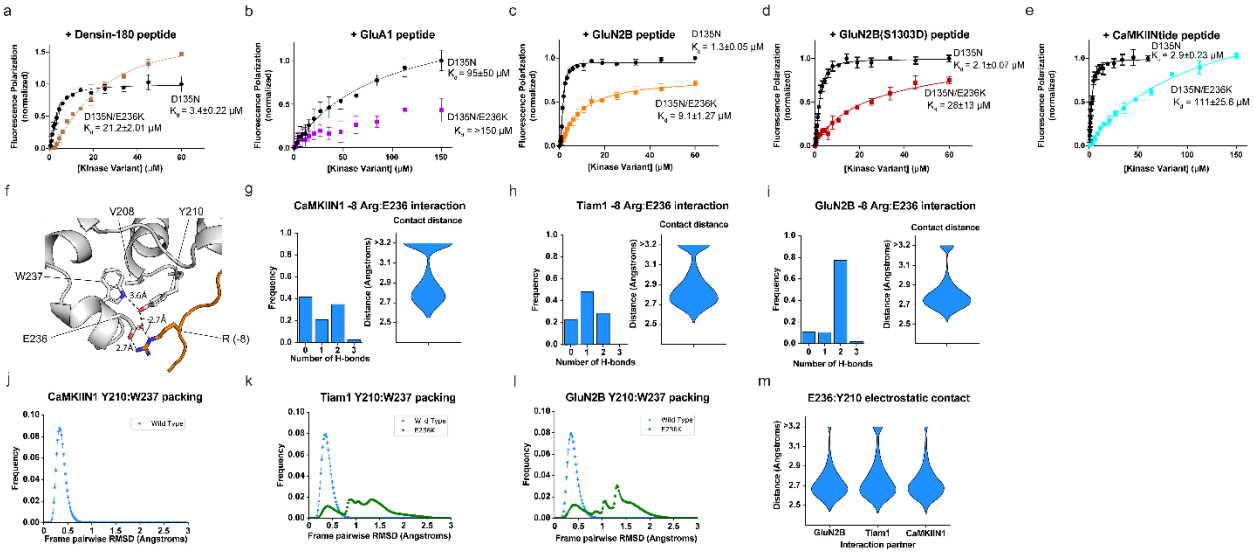

Figure S5. E236 forms a large hydrogen bond network within the kinase domain. FP measurements of the CaMKII kinase domain with E236K mutation binding to (a) Densin-180 (brown), (b) GluA1 (purple), (c) GluN2B (orange), (d) GluN2B (S1303D) (red), (e) CaMKIINtide (cyan) peptides. (f) Hydrogen bond network between W237, Y210, and E236 of CaMKII kinase domain and R(-8) of GluN2B peptide. (g-i) Electrostatic interactions between R(-8) of peptide and E236 in MD simulations. Histogram of the number of Hbonds (left) and distribution of contact distance (right) for (g) CaMKIIN1, (h) Tiam1, and (i) GluN2B. (j-l) RMDS histograms for hydrophobic packing of V208, Y210, and W237 in MD simulations of wild type kinase domain (blue) and kinase domain with E236K mutation (green) for (j) CaMKIIN1, (k) Tiam1, and (l) GluN2B. (m) Distance distributions for the electrostatic contact between E236 and Y210 in MD simulations of wild type kinase domain with GluN2B, Tiam1, and CaMKIIN1.

a

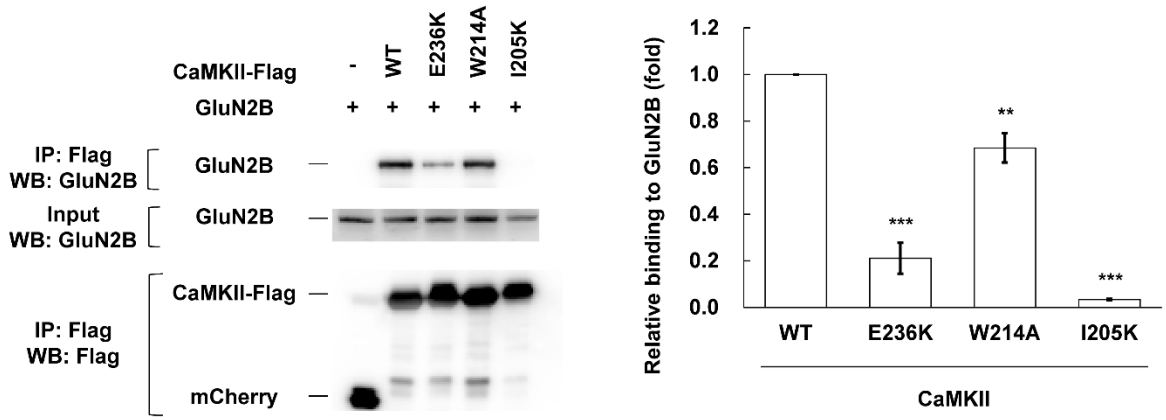

b

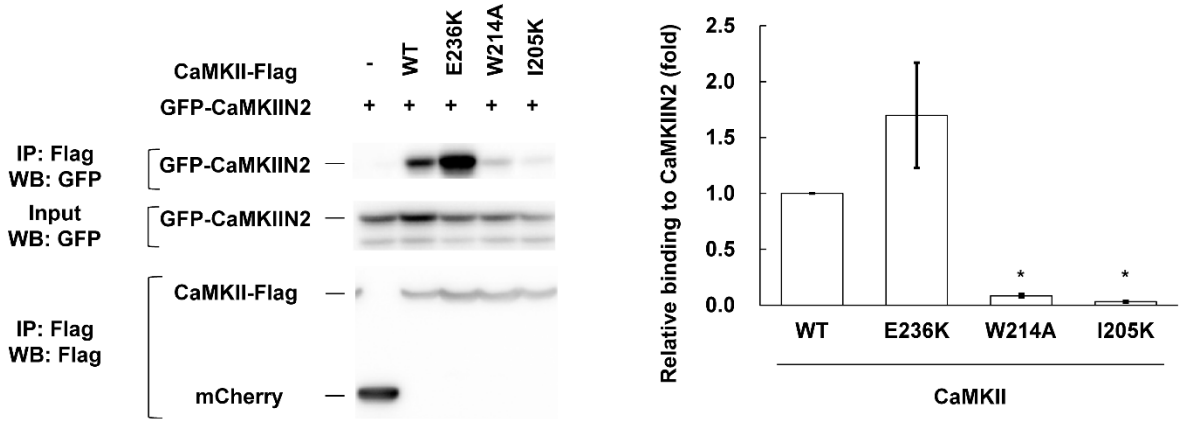

Figure S6. Effects of CaMKII mutations (E236K, W214A and I205K) on the interaction with full-length GluN2B and CaMKIIN2.
HEK293T cells were co-transfected with Flag-tagged CaMKII and GluN2B or EGFP-CaMKIIN2. Cell lysates were immunoprecipitated with Flag antibody, and samples were immunoblotted with GluN2B, GFP and Flag antibodies. Representative blots were shown in (a) GluN2B, and (b) CaMKIIN2. The amount of co-immunoprecipitated GluN2B or CaMKIIN2 was normalized by the amount in cell lysate and immunoprecipitated CaMKII. Quantification of the co-immunoprecipitation from 3 or 4 independent experiments were shown in a graph of (a) GluN2B (n=3) (b) CaMKIIN2 (n=4). *$p < 0.05$, **, < 0.01 and ***, < 0.001, compared to WT CaMKII; one-way ANOVA with the Shaffer's post hoc test comparisons. WT, wild type; IP, immunoprecipitation.

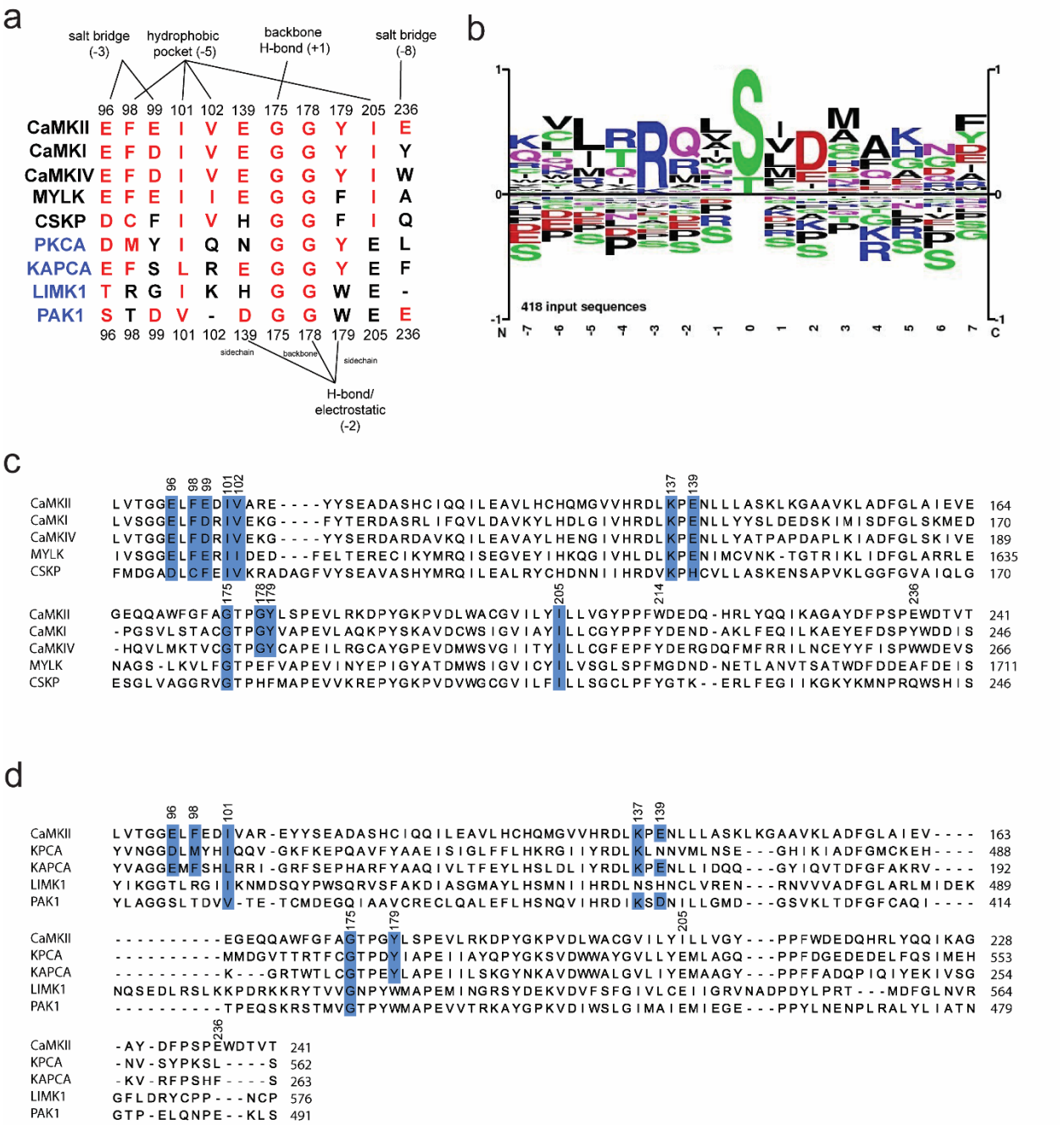

Figure S7. Multi-sequence alignment of kinase domains.
(a) Alignment of key residues involved in binding substrates across kinases from the Ca^{2+}/CaM family (black text) and four kinases from different families (blue text). PKCA and KAPCA (cAMP dependent kinase) belong to the AGC Ser/Thr family. LimK1 and Pak1 belong to TKL and STE Ser/Thr family. (b) The sequence logo for all previously identified substrates of CaMKII from the PhosphoSitePlus database with the phosphorylation site at the 0 position. Conserved residues are highlighted blue. (c) across Ca^{2+}/CaM family. (d) across different kinase families.

832
833 **Supplementary Table 1. ITC values for CaMKII kinase domain binding to interaction**
834 **partners**

In the cell	In the syringe	K_D (nM)	N	ΔH (kJ/mol)	-TΔS (kJ/mol)	Cell/Syringe concentration (μM)
CaMKII KD (D135N)	GluN2B	128±18.3	0.818±5.5 x 10^{-3}	-44.9±0.631	6.17	20/200
CaMKII KD (D135N)	Tiam1	1.15 x 10^3±90	0.795±7.1 x 10^{-3}	-86.9±1.5	53.5	20/200
CaMKII KD (D135N)	Densin-180	666±91.1	0.779±10^{-2}	-33.1±0.803	-1.57	20/200
CaMKII KD (D135N)	CaMKIIN2	56.4±12.5	0.992±6.4 x 10^{-3}	-33±0.384	-7.68	20/200
CaMKII KD (D135N)	GluA1	72 x 10^3±5.93 x 10^3	1	-20.4±0.889	-2.82	40/500
CaMKII KD (D135N/E236K)	CaMKIIN2	951±160	0.881±1.8 x 10^{-2}	-29.8±0.815	-4.07	20/200
CaMKII KD (D135N)	GluN2B (S1303D)	919±100	0.725±8.6 x 10^{-3}	-39±0.864	5.11	20/200
CaMKII KD (D135N)	Extended Syntide-2 (GRR-Syntide-2)	1.91 x 10^3±273	0.908±1.8 x 10^{-2}	-15.1±0.581	-17	20/200

835
836
837 **REFERENCES**
838

839 1. Lisman, J., R. Yasuda, and S. Raghavachari, *Mechanisms of CaMKII action in long-term*
840 *potentiation.* Nat Rev Neurosci, 2012. **13**(3): p. 169-82.
841 2. Malenka, R.C., et al., *An essential role for postsynaptic calmodulin and protein kinase*
842 *activity in long-term potentiation.* Nature, 1989. **340**(6234): p. 554-7.
843 3. Sloutsky, R. and M.M. Stratton, *Functional implications of CaMKII alternative splicing.*
844 Eur J Neurosci, 2020.
845 4. Erondu, N.E. and M.B. Kennedy, *Regional distribution of type II Ca2+/calmodulin-*
846 *dependent protein kinase in rat brain.* J Neurosci, 1985. **5**(12): p. 3270-7.

847 5. Lynch, M.A., *Long-term potentiation and memory.* Physiol Rev, 2004. **84**(1): p. 87-136.
848 6. Ishida, A. and H. Fujisawa, *Stabilization of Calmodulin-Dependent Protein-Kinase-Ii*
849 *through the Autoinhibitory Domain.* Journal of Biological Chemistry, 1995. **270**(5): p.
850 2163-2170.
851 7. Bayer, K.U., et al., *Interaction with the NMDA receptor locks CaMKII in an active*
852 *conformation.* Nature, 2001. **411**(6839): p. 801-5.
853 8. Bayer, K.U., et al., *Transition from reversible to persistent binding of CaMKII to*
854 *postsynaptic sites and NR2B.* J Neurosci, 2006. **26**(4): p. 1164-74.
855 9. Saneyoshi, T., et al., *Reciprocal Activation within a Kinase-Effector Complex Underlying*
856 *Persistence of Structural LTP.* Neuron, 2019. **102**(6): p. 1199-1210 e6.
857 10. Strack, S. and R.J. Colbran, *Autophosphorylation-dependent targeting of calcium/*
858 *calmodulin-dependent protein kinase II by the NR2B subunit of the N-methyl- D-*
859 *aspartate receptor.* J Biol Chem, 1998. **273**(33): p. 20689-92.
860 11. Strack, S., R.B. McNeill, and R.J. Colbran, *Mechanism and regulation of*
861 *calcium/calmodulin-dependent protein kinase II targeting to the NR2B subunit of the N-*
862 *methyl-D-aspartate receptor.* J Biol Chem, 2000. **275**(31): p. 23798-806.
863 12. Omkumar, R.V., et al., *Identification of a phosphorylation site for*
864 *calcium/calmodulindependent protein kinase II in the NR2B subunit of the N-methyl-D-*
865 *aspartate receptor.* J Biol Chem, 1996. **271**(49): p. 31670-8.
866 13. Walikonis, R.S., et al., *Densin-180 forms a ternary complex with the (alpha)-subunit of*
867 *Ca2+/calmodulin-dependent protein kinase II and (alpha)-actinin.* J Neurosci, 2001.
868 **21**(2): p. 423-33.
869 14. Jiao, Y., et al., *Characterization of a central Ca2+/calmodulin-dependent protein kinase*
870 *IIalpha/beta binding domain in densin that selectively modulates glutamate receptor*
871 *subunit phosphorylation.* J Biol Chem, 2011. **286**(28): p. 24806-18.
872 15. Mammen, A.L., et al., *Phosphorylation of the alpha-amino-3-hydroxy-5-*
873 *methylisoxazole4-propionic acid receptor GluR1 subunit by calcium/calmodulin-*
874 *dependent kinase II.* J Biol Chem, 1997. **272**(51): p. 32528-33.
875 16. Barria, A., V. Derkach, and T. Soderling, *Identification of the Ca2+/calmodulin-dependent*
876 *protein kinase II regulatory phosphorylation site in the alpha-amino-3-hydroxyl-5-*
877 *methyl-4-isoxazole-propionate-type glutamate receptor.* J Biol Chem, 1997. **272**(52): p.
878 32727-30.
879 17. Diering, G.H. and R.L. Huganir, *The AMPA Receptor Code of Synaptic Plasticity.* Neuron,
880 2018. **100**(2): p. 314-329.
881 18. Barria, A., et al., *Regulatory phosphorylation of AMPA-type glutamate receptors by CaM-*
882 *KII during long-term potentiation.* Science, 1997. **276**(5321): p. 2042-5.
883 19. Derkach, V., A. Barria, and T.R. Soderling, *Ca2+/calmodulin-kinase II enhances channel*
884 *conductance of alpha-amino-3-hydroxy-5-methyl-4-isoxazolepropionate type glutamate*
885 *receptors.* Proc Natl Acad Sci U S A, 1999. **96**(6): p. 3269-74.
886 20. Chao, L.H., et al., *Intersubunit capture of regulatory segments is a component of*
887 *cooperative CaMKII activation.* Nat Struct Mol Biol, 2010. **17**(3): p. 264-72.
888 21. Wang, C., et al., *A novel endogenous human CaMKII inhibitory protein suppresses tumor*
889 *growth by inducing cell cycle arrest via p27 stabilization.* J Biol Chem, 2008. **283**(17): p.
890 11565-74.

891 22. Zhang, J., et al., *Molecular cloning and characterization of a novel calcium/calmodulin-*
892 *dependent protein kinase II inhibitor from human dendritic cells.* Biochem Biophys Res
893 Commun, 2001. **285**(2): p. 229-34.
894 23. Chang, B.H., S. Mukherji, and T.R. Soderling, *Calcium/calmodulin-dependent protein*
895 *kinase II inhibitor protein: localization of isoforms in rat brain.* Neuroscience, 2001.
896 **102**(4): p. 767-77.
897 24. White, R.R., et al., *Definition of optimal substrate recognition motifs of Ca2+-calmodulin-*
898 *dependent protein kinases IV and II reveals shared and distinctive features.* J Biol Chem,
899 1998. **273**(6): p. 3166-72.
900 25. Songyang, Z., et al., *A structural basis for substrate specificities of protein Ser/Thr*
901 *kinases: primary sequence preference of casein kinases I and II, NIMA, phosphorylase*
902 *kinase, calmodulin-dependent kinase II, CDK5, and Erk1.* Mol Cell Biol, 1996. **16**(11): p.
903 6486-93.
904 26. Ishida, A., et al., *Critical amino acid residues of AIP, a highly specific inhibitory peptide of*
905 *calmodulin-dependent protein kinase II.* FEBS Lett, 1998. **427**(1): p. 115-8.
906 27. Stokoe, D., et al., *The substrate specificity and structure of mitogen-activated protein*
907 *(MAP) kinase-activated protein kinase-2.* Biochem J, 1993. **296 (Pt 3)**: p. 843-9.
908 28. Castro-Rodrigues, A.F., et al., *The Interaction between the Drosophila EAG Potassium*
909 *Channel and the Protein Kinase CaMKII Involves an Extensive Interface at the Active Site*
910 *of the Kinase.* J Mol Biol, 2018. **430**(24): p. 5029-5049.
911 29. Coultrap, S.J. and K.U. Bayer, *Improving a natural CaMKII inhibitor by random and*
912 *rational design.* PLoS One, 2011. **6**(10): p. e25245.
913 30. Yang, E. and H. Schulman, *Structural examination of autoregulation of multifunctional*
914 *calcium/calmodulin-dependent protein kinase II.* J Biol Chem, 1999. **274**(37): p. 26199-
915 208.
916 31. Rellos, P., et al., *Structure of the CaMKIIdelta/calmodulin complex reveals the molecular*
917 *mechanism of CaMKII kinase activation.* PLoS Biol, 2010. **8**(7): p. e1000426.
918 32. Rust, H.L. and P.R. Thompson, *Kinase consensus sequences: a breeding ground for*
919 *crosstalk.* ACS Chem Biol, 2011. **6**(9): p. 881-92.
920 33. Zha, M., et al., *Crystal structures of human CaMKIalpha reveal insights into the*
921 *regulation mechanism of CaMKI.* PLoS One, 2012. **7**(9): p. e44828.
922 34. Torres-Ocampo, A.P., et al., *Characterization of CaMKII alpha holoenzyme stability.*
923 Protein Science, 2020. **29**: p. 1524-1534.
924 35. Endicott, J.A., M.E. Noble, and L.N. Johnson, *The structural basis for control of eukaryotic*
925 *protein kinases.* Annu Rev Biochem, 2012. **81**: p. 587-613.
926 36. Robison, A.J., et al., *Differential modulation of Ca2+/calmodulin-dependent protein*
927 *kinase II activity by regulated interactions with N-methyl-D-aspartate receptor NR2B*
928 *subunits and alpha-actinin.* J Biol Chem, 2005. **280**(47): p. 39316-23.
929 37. Mao, L.M., et al., *Phosphorylation and regulation of glutamate receptors by CaMKII.*
930 Sheng Li Xue Bao, 2014. **66**(3): p. 365-72.
931 38. Hosokawa, T., et al., *Stoichiometry and phosphoisotypes of hippocampal AMPA-type*
932 *glutamate receptor phosphorylation.* Neuron, 2015. **85**(1): p. 60-67.
933 39. McCoy, A.J., et al., *Phaser crystallographic software.* J Appl Crystallogr, 2007. **40**(Pt 4): p.
934 658-674.

40. Murshudov, G.N., A.A. Vagin, and E.J. Dodson, *Refinement of macromolecular structures by the maximum-likelihood method.* Acta Crystallogr D Biol Crystallogr, 1997. **53**(Pt 3): p. 240-55.
41. Winn, M.D., et al., *Overview of the CCP4 suite and current developments.* Acta Crystallogr D Biol Crystallogr, 2011. **67**(Pt 4): p. 235-42.
42. Eastman, P., et al., *OpenMM 4: A Reusable, Extensible, Hardware Independent Library for High Performance Molecular Simulation.* J Chem Theory Comput, 2013. **9**(1): p. 461-469.
43. Pall, S., et al., *Tackling Exascale Software Challenges in Molecular Dynamics Simulations with GROMACS.* Solving Software Challenges for Exascale, 2015. **8759**: p. 3-27.
44. Huang, J., et al., *CHARMM36m: an improved force field for folded and intrinsically disordered proteins.* Nat Methods, 2017. **14**(1): p. 71-73.
45. Jorgensen, W.L., et al., *Comparison of Simple Potential Functions for Simulating Liquid Water.* Journal of Chemical Physics, 1983. **79**(2): p. 926-935.
46. Hess, B., *P-LINCS: A Parallel Linear Constraint Solver for Molecular Simulation.* J Chem Theory Comput, 2008. **4**(1): p. 116-22.
47. Feenstra, K.A., B. Hess, and H.J.C. Berendsen, *Improving efficiency of large time-scale molecular dynamics simulations of hydrogen-rich systems.* Journal of Computational Chemistry, 1999. **20**(8): p. 786-798.
48. Essmann, U., et al., *A Smooth Particle Mesh Ewald Method.* Journal of Chemical Physics, 1995. **103**(19): p. 8577-8593.
49. Bussi, G., D. Donadio, and M. Parrinello, *Canonical sampling through velocity rescaling.* J Chem Phys, 2007. **126**(1): p. 014101.
50. Parrinello, M. and A. Rahman, *Polymorphic Transitions in Single-Crystals - a New Molecular-Dynamics Method.* Journal of Applied Physics, 1981. **52**(12): p. 7182-7190.
51. Larsson, P., R.C. Kneiszl, and E.G. Marklund, *MkVsites: A tool for creating GROMACS virtual sites parameters to increase performance in all-atom molecular dynamics simulations.* J Comput Chem, 2020. **41**(16): p. 1564-1569.
52. McGibbon, R.T., et al., *MDTraj: A Modern Open Library for the Analysis of Molecular Dynamics Trajectories.* Biophys J, 2015. **109**(8): p. 1528-32.
53. Barker, S.C., et al., *Characterization of pp60c-src tyrosine kinase activities using a continuous assay: autoactivation of the enzyme is an intermolecular autophosphorylation process.* Biochemistry, 1995. **34**(45): p. 14843-51.